

# JGR Solid Earth

## RESEARCH ARTICLE

10.1029/2023JB028314

### Key Points:

- Paleomagnetic dating of 12 Etna Holocene flank lava flows provided 40%–90% refinement of independent age constraints for 10 eruptions
- At Etna, where best method pre-requisites are satisfied, paleomagnetic dating provides singular age solutions for ca. 30% of the dated flows
- Paleomagnetism reduce by more than 40%–50% the eruptions' age windows for flows with independent age intervals lower than 7,000 years

### Supporting Information:

Supporting Information may be found in the online version of this article.

### Correspondence to:

A. Magli,  
[andrea.magli@uniroma3.it](mailto:andrea.magli@uniroma3.it)

### Citation:

Magli, A., Speranza, F., Branca, S., Corsaro, R. A., Coltellini, M., Malagutti, A. B., & Giordano, G. (2024). Testing paleomagnetic dating on pre-historic flank eruptions from SE slope of Etna Volcano. *Journal of Geophysical Research: Solid Earth*, 129, e2023JB028314. <https://doi.org/10.1029/2023JB028314>

Received 20 NOV 2023

Accepted 9 AUG 2024

### Author Contributions:

**Conceptualization:** Fabio Speranza, Stefano Branca, Rosa Anna Corsaro, Guido Giordano  
**Data curation:** Andrea Magli  
**Formal analysis:** Andrea Magli, Fabio Speranza, Arianna Beatrice Malagutti  
**Investigation:** Andrea Magli, Fabio Speranza, Stefano Branca, Mauro Coltellini, Arianna Beatrice Malagutti  
**Project administration:** Guido Giordano  
**Resources:** Fabio Speranza  
**Supervision:** Fabio Speranza, Stefano Branca, Guido Giordano  
**Validation:** Fabio Speranza, Stefano Branca, Guido Giordano  
**Visualization:** Andrea Magli, Rosa Anna Corsaro, Guido Giordano  
**Writing – original draft:** Andrea Magli

## Testing Paleomagnetic Dating on Pre-Historic Flank Eruptions From SE Slope of Etna Volcano

Andrea Magli<sup>1,2</sup> , Fabio Speranza<sup>2</sup> , Stefano Branca<sup>3</sup> , Rosa Anna Corsaro<sup>3</sup> , Mauro Coltellini<sup>3</sup> , Arianna Beatrice Malagutti<sup>2,3</sup> , and Guido Giordano<sup>1,4</sup> 

<sup>1</sup>Dipartimento di Scienze, Università degli Studi di Roma Tre, Roma, Italy, <sup>2</sup>Istituto Nazionale di Geofisica e Vulcanologia, Roma, Italy, <sup>3</sup>Istituto Nazionale di Geofisica e Vulcanologia, Osservatorio Etneo-Sezione di Catania, Catania, Italy,

<sup>4</sup>Consiglio Nazionale delle Ricerche – IGAG, Roma, Italy

**Abstract** During the last 20 kyr, the Etna volcano has been characterized by almost continuous summit eruptions and by less frequent—yet definitely more destructive—flank eruptions issuing at <1,000 m asl altitudes and reaching the Ionian Sea. The chronological framework of pre-historic (pre-2,750 yr BP) flank eruptions is supported only by few radiometric and paleomagnetic ages. Here we paleomagnetically investigated 15 Holocene lava flows from SE Etna lower slopes and dated 12 of them. Paleomagnetic dating at Etna relies on best method pre-requisites: European location where reference geomagnetic models are well defined, and detailed stratigraphic evidence is available. We sampled 45 sites (450 oriented cores) from lavas loosely constrained in the 19,000–2,000 yr BP age window. Ten eruptions yielded a minimum 40% refinement with respect to initial age constraints, with four lava flows achieving refinement up to 90%. We obtained 620–1,398 yr (998 yr on average) dating accuracy for three flows bracketed in relatively short (1,398–1,644 yr) independent age constraints. By contrast, five flows characterized by longer 6,567–7,439 yr initial age windows yielded multiple age solutions. Finally, four lava flows with 1,644–6,567 yr-long initial age windows were tightly dated with 120–680 yr age ranges. We conclude that at volcanoes where best paleomagnetic dating pre-requisite are fulfilled, singular solutions are expected for 30% of the analyzed flows and, significant refinements for the others. Seven kyr seems to represent an independent age window threshold length to get or not significant dating refinements.

**Plain Language Summary** Reconstructing a volcano's past eruptive activity, particularly over the last few centuries or millennia, is essential for conducting comprehensive long-term hazard assessments. Mount Etna (Sicily, Italy) is an active basaltic volcano characterized by infrequent but highly destructive flank eruptions whose lava flows historically have impacted the populated lower slopes of the volcano. As the timing of the Etna prehistoric flank eruptions currently remains poorly determined, we used the paleomagnetic dating method, which offers a high level of precision that is challenging to achieve using alternative radiometric techniques in Holocene (i.e., last ca. 14 ky) basaltic products. Out of a total of 15 Holocene lava flows investigated, which are distributed over the Etna SE lower slopes, we paleomagnetically dated 12 flows by comparing their flow-mean paleomagnetic directions with Paleo-Secular Variation (PSV) reference curves, the latter showing the changes of the geomagnetic field over time. Our data show that for most of the studied eruptions, the paleomagnetic ages significantly reduce their independent age constraints, thus providing an improvement to the understanding of Etna Holocene eruptive activity.

## 1. Introduction

The detailed reconstruction of the past activity of a volcano (especially of the last few centuries or millennia) is fundamental for long-term hazard assessment (Connor et al., 2015). Hazards at explosive volcanoes are associated mostly with pyroclastic fall and flow processes (Biass et al., 2016; Jenkins et al., 2015; Selva et al., 2019), which represent the most fatal volcanic events. However, basaltic volcanoes that usually erupt effusively, may be highly hazardous for human communities that inhabit their lower slopes when infrequent, but very destructive flank eruptions originate at lower altitudes. In recent years, the large lava flows produced by such types of events have caused severe damages to buildings and infrastructures, such as during the 1943–1952 Paricutin (Mexico; Becerril et al., 2021; Krauskopf, 1948a, 1948b), the 2018 Hawaii (Meredith et al., 2022; Neal et al., 2019; Patrick et al., 2019), and the 2021 La Palma (Canary Islands) eruptions (Bonadonna et al., 2022; Carracedo et al., 2022; Di Fiore et al., 2023). Rarely, where conditions of low viscosity favored extremely high flow velocities, lava

**Writing – review & editing:**

Fabio Speranza, Stefano Branca, Rosa Anna Corsaro, Arianna Beatrice Malaguti, Guido Giordano

flows have also caused fatalities (e.g., the 2002 and 2021 Nyiragongo eruptions: Barrière et al., 2022; Komorowski, 2002; Smittarello et al., 2022; Tedesco et al., 2007).

Similar hazards also affect Mount Etna (Italy), the most active basaltic volcano in the Mediterranean area and one of the most active in the world (Branca, Coltelli, Groppelli, et al., 2011). Although summit eruptions frequently characterize the Etna eruptive activity, numerous flank eruptions also issued from fissures opened along the lower volcano slopes in historical times (Andronico et al., 2021; Branca & Abate, 2019; Branca & Del Carlo, 2005; De Beni et al., 2021), as well as during the Holocene (Figure 1; Branca, Coltelli, Groppelli, et al., 2011; Branca et al., 2019; Magli et al., 2022; Malaguti et al., 2023). The most recent flank eruption occurred in the lower SE flank in AD 1669, producing the large scoria cone of Monti Rossi and a voluminous ( $607 \pm 105 \times 10^6 \text{ m}^3$ , Branca et al., 2013) lava flow field that dramatically impacted several villages and cultivated areas of the SE volcano flank and partially destroyed the Catania town, entering the Ionian Sea (Branca et al., 2013; Branca, Azzaro, et al., 2015).

Clearly, defining the frequency of Etna flank eruptions during the geological past is a fundamental issue for evaluating volcanic hazard. The  $^{14}\text{C}$ , K/Ar, and  $^{40}\text{Ar}/^{39}\text{Ar}$  isotopic methods are the prevailing dating techniques used to obtain eruption absolute ages. However, radiometric methods have some significant drawbacks: (a) depending on laboratory procedures of dating method and on the type of sampled rock (e.g., basaltic lavas containing very low potassium), K/Ar or  $^{40}\text{Ar}/^{39}\text{Ar}$  dating can be either impossible or provide highly uncertain results (e.g., Calvari et al., 2011; Renne et al., 1997; Risica et al., 2019; Takaoka, 1989; Wijbrans et al., 2011); (b) suitable organic material from paleosols underlying lavas for  $^{14}\text{C}$  dating may be sparse, or even lacking in arid climate conditions, and dating may be biased by ambient carbon contamination (e.g., Bruns et al., 1980; Carracedo et al., 2007; Christie, 2018; Pasquier-Cardin et al., 1999; Saupé et al., 1980).

In order to overcome the limitations of these classic radiometric methods for the dating of recent basaltic lavas, during the last few decades many volcanoes worldwide have been investigated using paleomagnetism, which has proved to be a useful dating tool for volcanic products emplaced during the Holocene (Branca, Condomines, & Tanguy, 2015; Gonzalez et al., 1997; Greve & Turner, 2017; Jurado-Chichay et al., 1996; Lanza & Zanella, 2003; Mahgoub, Böhnle, Siebe, & Chevrel, 2017; Mahgoub, Böhnle, Siebe, Salinas, & Guilbaud, 2017; Magli et al., 2022; Malaguti et al., 2022, 2023; Pavón-Carrasco & Villasante-Marcos, 2010; Pinton et al., 2018; Risica et al., 2019, 2020, 2022; Speranza et al., 2004, 2006, 2008; Tanguy et al., 2003, 2007; Thompson & Turner, 1985; among many others). Dating is achieved by comparing paleomagnetic directions (and intensity, where available) from volcanics with models of the Paleo-Secular Variation (PSV) of the geomagnetic field. The reliability and accuracy of paleomagnetic dating are controversial, and depend upon local magnetic anomalies, possible unrecognized rock tilt, and—most importantly—upon localities such as Europe where a wealth of independent reference PSV data are available (e.g., Speranza et al., 2006).

This work focuses on the reliability and accuracy of the paleomagnetic dating method when applied to lavas issued by flank eruptions along the SE Mount Etna slopes between 14 and 2 ka ago. We show that—even at volcanoes fulfilling best method pre-requisites such as Etna—paleomagnetic dating yields singular solutions for about 30% of flows if  $>1,500$  years independent age constraints are considered.

## 2. Geological Background

Etna is one of the most monitored and studied volcanoes in the world. The combination of geological data, historical documents, archeological findings, and radiometric age determinations form the basis of the reconstructed stratigraphic setting of the recent geological map of Etna at 1:50,000 scale (Branca, Coltelli, & Groppelli, 2011; Branca, Coltelli, Groppelli, et al., 2011; De Beni et al., 2011). The radiometric methods generally used to date the Etna eruptive products are K/Ar and  $^{40}\text{Ar}/^{39}\text{Ar}$  (for volcanics tens of kyr old), AMS  $^{14}\text{C}$ , and  $^{226}\text{Ra}/^{230}\text{Th}$  (for products of the last 19 ky). From here on, K/Ar,  $^{40}\text{Ar}/^{39}\text{Ar}$ ,  $^{226}\text{Ra}/^{230}\text{Th}$ , archeological, and previous paleomagnetic ages will be reported in calendar years. We recalibrated published radiocarbon ages to BC/AD ages using CALIB8.1.0 (Stuiver et al., 2021) and the IntCal20 calibration curve (Reimer et al., 2020), and subsequently converted them to yr BP (where Present is AD 1,950) by subtracting the AD year from 1,950 AD or adding the BC year. The same approach of conversion in yr BP was used for the other radiometric, archeological, and paleomagnetic ages.

Mount Etna is a large basaltic composite volcano, with an  $1,178 \text{ km}^2$  area, maximum base length of 45 km, and a 3,357 m asl altitude (Figure 1). The volcanic edifice is the result of a complex geological evolution that started at

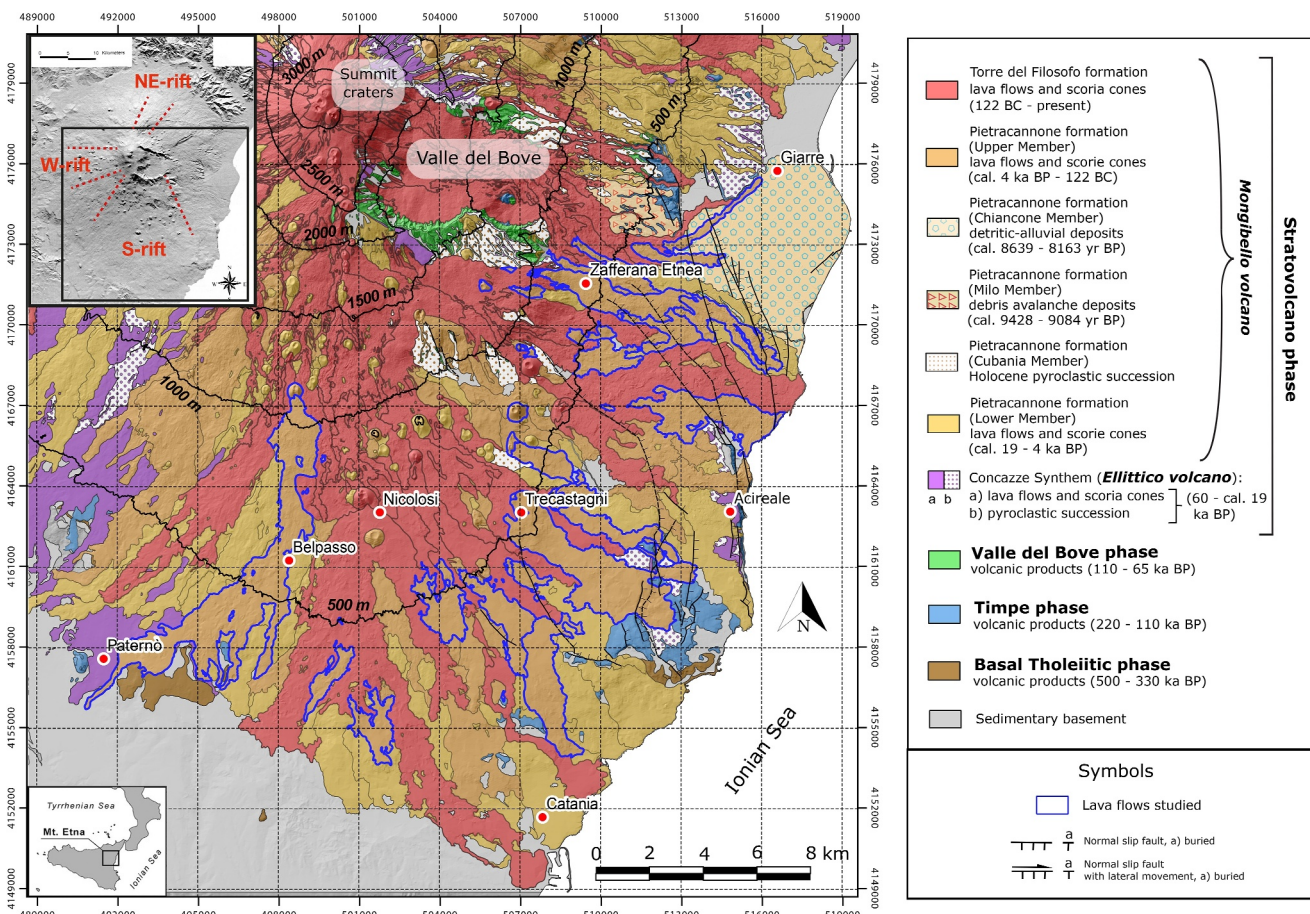


**Figure 1.** Simplified geological map of the lower southeastern flank of Monte Etna volcano (modified from Branca, Coltelli, Groppelli, et al., 2011) showing the studied lava flows outlined in blue.

around 500 ka ago in a submarine environment (Branca, Coltelli, & Groppelli, 2011; Branca, Coltelli, Groppelli, et al., 2011; De Beni et al., 2011). The last 60 ky of the Etna eruptive history were characterized by both effusive and explosive summit eruptions, ranging from strombolian to Plinian in intensity, and effusive to strombolian flank eruptions (Stratovolcano phase; Branca, Coltelli, Groppelli, et al., 2011). During the last few millennia, the lower sectors of the volcano have been affected by several flank eruptions linked to the activity of the three main magma intrusion zones, also called “rifts”: S, NE, and W rifts (Azzaro et al., 2012; Figure 1). In particular, the Etna southeastern lower flank has been repeatedly affected by the S rift activity (Figure 1), and has yielded the largest number of flank eruptions in historical times (Andronico et al., 2021; Behncke et al., 2005; Branca & Abate, 2019; Branca & Del Carlo, 2005).

## 2.1. Geological Setting of SE Etna Lower Slopes

The oldest eruptive products of the Etna lower south-eastern slopes rest on the Early Middle Pleistocene marly clays and belong to the Basal Tholeiitic and Timpe phases (Branca, Coltelli, & Groppelli, 2011; Branca, Coltelli, Groppelli, et al., 2011; Figure 1), dated at ca. 500 and 330 ka ago and from 220 to 110 ka ago, respectively (De Beni et al., 2011). In the area of the Valle del Bove depression, several polygenic volcanic centers formed between 110 and 65 ka ago (Valle del Bove phase; Branca, Coltelli, Groppelli, et al., 2011; De Beni et al., 2011), whose volcanic products are visible along the inner walls of the Valle del Bove (Figure 1). Several lava flows and pyroclastic successions from the Ellittico volcano, dated from 60 to 19 ka ago (Concasse Synthem, Stratovolcano Phase of Branca, Coltelli, Groppelli, et al., 2011; De Beni et al., 2011; Figure 1) also crop out. The lower eastern slope presents widespread volcanoclastic deposits (i.e., the Milo and Chiancone members by Branca, Coltelli, Groppelli, et al., 2011; Figure 1) related to sector collapses of the Etna eastern flank that occurred starting from

cal. 9,428–9,084 yr BP (AMS radiocarbon age by Malaguti et al., 2023) and gradually generated the wide depression of the Valle del Bove.

Most of the lower SE slope is formed by scoria cones, lava flows, and pyroclastic fallout deposits younger than 19 ka ago (“Mongibello volcano,” Stratovolcano Phase in Branca, Coltell, Groppelli, et al., 2011). Given the paucity of available isotopic dating (K/Ar and  $^{40}\text{Ar}/^{39}\text{Ar}$  radiometric methods can be hardly used due to K paucity in the magmas), some Holocene tephra layers were used as markers to better constrain the age range of the lava flows emplaced during this time span. Among these tephra, three pyroclastic fallout deposits, with an east to southeast dispersal, were erupted at cal. 18,862–18,636 yr BP AMS age (caldera-forming final eruption of Ellittico volcano; D1a tephra layer of Coltell et al., 2000), cal. 4,523–4,230 yr BP  $^{14}\text{C}$  age (picritic sub-Plinian eruption; FS tephra layer of Coltell et al., 1998, 2000), and at 122 BC (a historically documented basaltic Plinian eruption; FG tephra layer of Coltell et al., 1998, 2000), respectively. Based on these tephra layers the products between ca. 19 ka and 4 ka ago have been grouped in the Lower Member of the Pietracannone Formation (Branca, Coltell, Groppelli, et al., 2011; Figure 1), whereas those comprised between 4 ka ago and 122 BC have been assigned to the Upper Member of Pietracannone Formation (Branca, Coltell, Groppelli, et al., 2011; Figure 1). It must be noted that the BP ages reported here for D1a and FS tephra layers are different from those indicated in previous works (e.g., Magli et al., 2022) for the same layers, that is, ca. 15 ka ago and  $3,930 \pm 60$  yr BP, respectively, which are the conventional radiocarbon ages (CRA) of Coltell et al. (2000) that were not recalibrated.

## 2.2. Holocene Etna Activity

The Etna eruptive activity during the historical period (last 2,750 years) has been extensively investigated by correlating stratigraphic evidence, radiometric/paleomagnetic data, and historical accounts (Branca & Abate, 2019; Branca, Condomines, & Tanguy, 2015; Speranza et al., 2006; Tanguy et al., 2007, 2012). Moreover, radiometric dating of volcanic rocks and underlying paleosols (e.g.,  $^{14}\text{C}$ , K/Ar,  $^{40}\text{Ar}/^{39}\text{Ar}$ , and  $^{226}\text{Ra}/^{230}\text{Th}$ ) as well as archeological findings (Branca et al., 2021) have been used to reconstruct the chronostratigraphy of pre-historical Holocene (i.e., 2.7–19 ka ago; see Section 2.1) volcanic deposits. However, a precise chronological reconstruction of the pre-historic eruptions is still lacking.

Several paleomagnetic investigations have been carried out at Mount Etna to date flank eruptions of the past 2,750 years (Tanguy et al., 1985, 2003, 2007, 2012; Branca, Coltell, & Groppelli, 2011; Branca, Coltell, Groppelli, et al., 2011; Chevallier, 1925; Incoronato et al., 2002; Rolph & Shaw, 1986; Speranza et al., 2006). However, concerning the pre-historic period, paleomagnetic dating was applied only to (a) the lower Holocene Alcantara flows on the N Etna margin (Branca et al., 2019), (b) two flows lying below the Catania town along the Ionian Sea (Magli et al., 2022), and (c) several lava flows emplaced within the Valle del Bove depression after its collapse (Malaguti et al., 2023).

The 15 Holocene lava flows selected in this work (Figure 2) belong to the Upper Member of Pietracannone Formation (between 4 ka ago and 122 BC according to Branca, Coltell, Groppelli, et al., 2011). However, a stratigraphic contact between the two cal. 4,000 yr BP/122 BC tephra layers and most of our studied lava flows is lacking, due to limited distribution of such layers along the Etna SE lower slopes. Thus, stratigraphic, radiometric, and archeological data acquired recently were considered to get age constraints of the studied flows. The “independent age constraints,” ranging from 12,000 BC (13,950 yr BP) to AD 750 (1,255 yr BP), are the time ranges within which the paleomagnetic directions were compared with PSV curves for dating. More details on the initial age constraints, along with information on the lava flows morphological features and pyroclastic/epiclastic deposits (taken from the Electronic Supplementary Materials of Branca, Coltell, Groppelli, et al., 2011) are reported in Table 1 and Text S1 in Supporting Information S1. The order through which the investigated flows are shown in this work follows both a spatial (from W to E side of the southeastern Etna lower flank) and temporal criterion (i.e., the stratigraphic order for each lava flows stack).

## 3. Paleomagnetic Dating Method

### 3.1. Validity and Limits

Paleomagnetic dating is achieved by comparing the paleomagnetic directions (and intensities, if available) recorded by naturally magnetized materials (geologic or archeological), with the PSV curve(s) of the geomagnetic field (Greve et al., 2016; Juárez-Arriaga et al., 2018; Magli et al., 2022; Malaguti et al., 2022; Pinton et al., 2018;

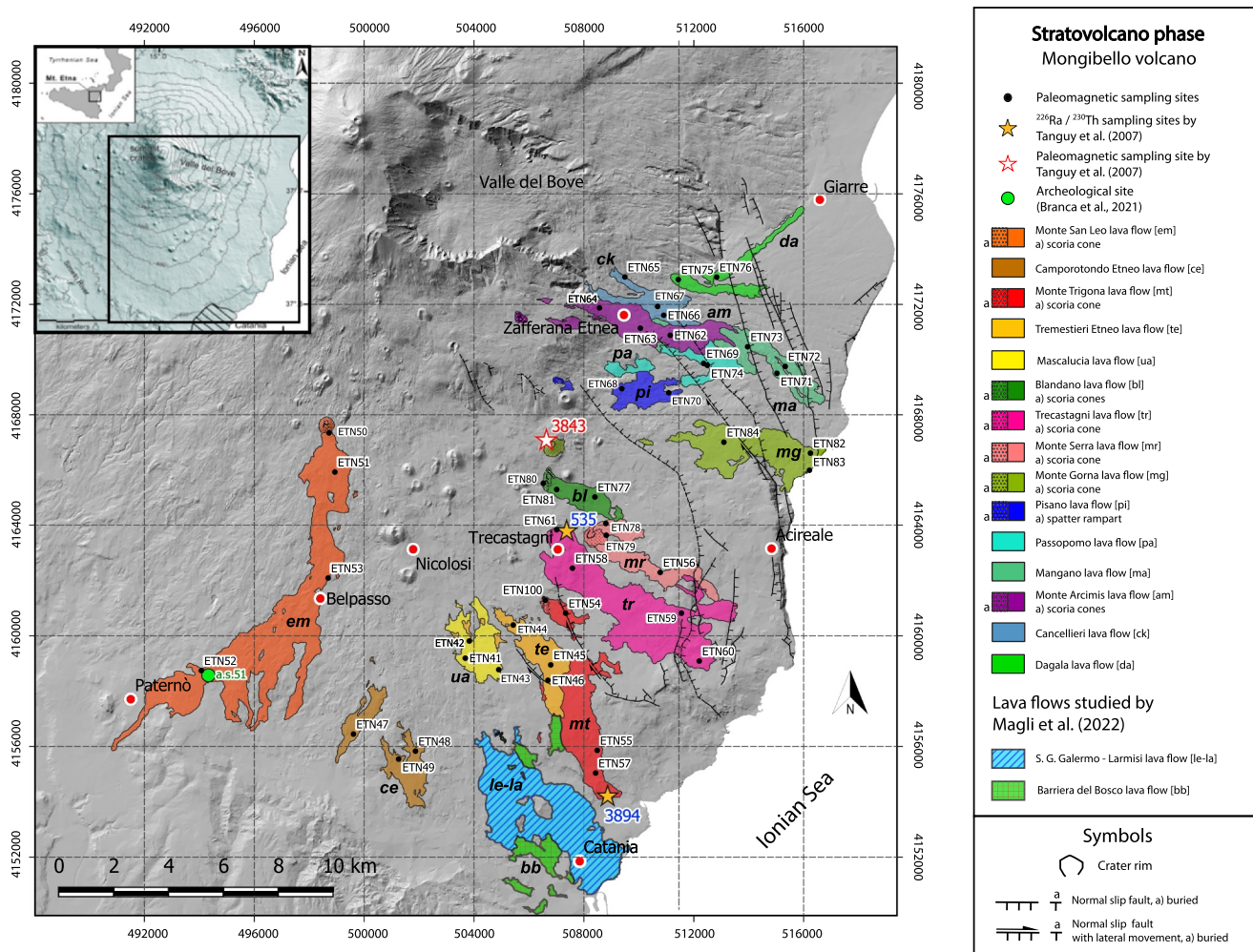


**Figure 2.** Sketch map of the lower southeastern flank of Mount Etna volcano showing the studied lava flows, and the paleomagnetic sampling sites. The lava flows analyzed by Magli et al. (2022) are also shown. Stars represent  $^{226}\text{Ra}/^{230}\text{Th}$  (yellow filling and black contour) and paleomagnetic (white filling and red contour) sampling sites, respectively, by Tanguy et al. (2007). The black circle with green filling is the archeological site studied by Branca et al. (2021). Lava flows abbreviations are reported on map and legend. The shaded relief image was derived from the 10-m resolution TINITALY DEM (Tarquini & Nannipieri, 2017).

Risica et al., 2020; Speranza et al., 2004, 2006; Tanguy et al., 2012; Villasante-Marcos & Pavón-Carrasco, 2014). The latter are the age-calibrated directional (and intensity) Holocene trends predicted by either PSV reference curves obtained in a given region and relocated to the site by pole method or by PSV spherical harmonic models yielding geomagnetic directions expected at the study area. PSV curves and models are built by compiling and modeling paleomagnetic data from well-dated volcanic rocks, heated archeological artifacts, and sedimentary cores drilled in lacustrine post-glacial successions (Ali et al., 1999; Constable et al., 2016; Corkill & Turner, 2022; Greve et al., 2016; Nilsson et al., 2014; Pavón-Carrasco & Villasante-Marcos, 2010; Pavón-Carrasco et al., 2014, 2021; Tanguy et al., 2003; Turner & Thompson, 1981, 1982). Due to the occurrence of non-dipolar geomagnetic field characteristics, PSV data have regional validity, so that data from other continents cannot be used. Most of the reference data used here were gathered and/or compiled during the past decades in Europe (e.g., Carrancho et al., 2013; Gallet et al., 2002; Kovacheva et al., 2014; Speranza et al., 2008; Tema & Lanos, 2021; Thompson & Turner, 1985).

The paleomagnetic dating method has some unquestionable advantages (it can be applied on whole rock and on all lava types), but also some limitations. First, at a given locality similar geomagnetic directions may re-occur over time (Figure 3), implying that a paleomagnetic direction may correspond to several possible ages when wide (i.e., several millennia) independent age constraints are given. Second, reference PSV data are abundant in Europe yet more scarce or even absent in other world regions, implying that a high degree of precision of the paleomagnetic

**Table 1**  
*Mean Paleomagnetic Directions From the Lower Southeastern Slopes of Mount Etna, Independent Age Constraints (Extrapolated From Archeological, Geochronologic, and Geologic Evidence), and Inferred Ages*

Volcanic unit	Site	n/N	D°	I°	k	$\alpha_{95}^{\circ}$	Method	Age constraint (yr BP)	Inferred age (yr BP)
<b>Monte San Leo lava flow</b>	ETN50	9/10	346.7	50.0	108.9	5.0			
	ETN51*	10/10	325.9	53.6	27.77	9.3			
	ETN52*	10/10	21.2	42.2	3.97	27.9	AMS <sup>a</sup>		
	ETN53	10/10	352.6	54.6	110.7	4.6			
Monte San Leo lava flow (flow-mean made by site-mean)	ETN50 + ETN53	2/2	349.5	52.3	384.9	12.8	Archeological finds <sup>b</sup>	Younger boundary: 7,650–6,450 (5,700– 4,500 BC)	10,720–10,230 9,420–8,890 8,190–7,350
Monte San Leo lava flow (flow-mean made by ChRM <sup>s</sup> )		<b>19/40</b>	<b>349.6</b>	<b>52.4</b>	<b>100.6</b>	<b>3.4</b>			
<b>Camporotondo Etneo lava flow</b>	ETN47	8/10	354.2	52.9	142.0	4.7	Below Monpilieri flow		18,862–13,950
	ETN48*	10/10	353.0	16.0	5.18	23.5			
	ETN49	10/10	6.4	50.4	106.9	4.7	AMS <sup>a</sup>	Older boundary: cal. 18,862–18,636 (cal. 16,912–16,686 BC)	13,710–13,060 11,020–10,810
Camporotondo Etneo lava flow	ETN47 + ETN49	2/2	0.5	51.8	207.3	17.4			
Camporotondo Etneo lava flow (flow-mean made by site-mean)		<b>18/30</b>	<b>1.2</b>	<b>51.7</b>	<b>96.4</b>	<b>3.5</b>	Paleomagnetic dating (Monpilieri flow) <sup>c</sup>	Younger boundary: 2,350–1,950	5,510–5,360 5,170–3,480 1,970–1,950
Camporotondo Etneo lava flow (flow-mean made by ChRM <sup>s</sup> )									
<b>Monte Trigona lava flow</b>	ETN54*	10/10	327.7	65.9	160.1	3.8	$^{226}\text{Ra}/^{230}\text{Th}$ <sup>d</sup>	Older - Younger boundary: <b>5,410–3,860</b>	5,410–5,390 5,130–4,790 (4,790–4,330) (4,060–4,000)
	ETN55	9/10	355.0	54.5	210.2	3.6			
	ETN57	10/10	354.3	49.6	133.24	4.2			
	ETN100	10/10	1.0	49.6	97.22	4.9			
	ETN55 + ETN57 + ETN100	3/3	356.8	51.3	488.73	5.6			
Monte Trigona lava flow (flow-mean made by site-mean)		<b>29/40</b>	<b>356.8</b>	<b>51.2</b>	<b>117.93</b>	<b>2.5</b>			
Monte Trigona lava flow (flow-mean made by ChRM <sup>s</sup> )									
<b>Tremestieri Etneo lava flow</b>	ETN44*	10/10	14.2	66.3	27.72	9.3	Above MonteTrigona and S. G. Galermo– Larmisi flows		
	ETN45	3/10	351.3	60.6	327.5	6.8			(5,500–5,410) 4,970–4,790
	ETN46	10/10	348.1	61.1	182.6	3.6			

**Table 1**  
*Continued*

Volcanic unit	Site	n/N	D°	I°	k	$\alpha_{95}^{\circ}$	Method	Age constraint (yr BP)	Inferred age (yr BP)
Tremestieri Etneo lava flow (flow-mean made by site-mean)	ETN45 + ETN46	2/2	349.7	60.9	4,902.8	3.6	Paleomagnetic dating (S.G. Galermo-Larmisi flow) <sup>c</sup>	Older boundary: <b>5,494–5,387</b>	
Tremestieri Etneo lava flow (flow-mean made by ChRMs)	<b>13/30</b>	<b>348.8</b>	<b>61.0</b>	<b>212.9</b>	<b>2.8</b>	$^{226}\text{Ra}/^{230}\text{Th}$ (Mascalucia flow) <sup>c</sup>	Younger boundary: 6,220–3,850		
Mascalucia lava flow	ETN41	10/10	3.8	49.2	178.1	3.6	Above Tremestieri Etneo and S.G. Galermo-Larmisi flows		<sup>a</sup>
	ETN42	9/10	353.7	56.4	72.5	6.1		(5,480–5,390) (5,130–4,970)	
Mascalucia lava flow (flow-mean made by site-mean)	ETN43	10/10	353.9	51.0	216.3	3.3	Paleomagnetic dating (S.G. Galermo-Larmisi flow) <sup>e</sup>	Older boundary: <b>5,494–5,387</b>	4,970–4,320
Mascalucia lava flow (flow-mean made by site-mean) + ETN42 + ETN43	ETN41	3/3	357.4	52.3	244.1	7.9			
Mascalucia lava flow (flow-mean made by ChRMs)	<b>29/30</b>	<b>357.5</b>	<b>52.1</b>	<b>99.4</b>	<b>2.7</b>	$^{226}\text{Ra}/^{230}\text{Th}$ <sup>c</sup>	Younger boundary: 6,220–3,850	4,090–3,990	
Blandano lava flow	ETN77	7/10	12.8	58.3	113.2	5.7			18,862–13,950
	ETN80	10/10	11.7	53.7	242.8	3.1		<sup>a</sup>	
Blandano lava flow (flow-mean made by site-mean)	ETN81	10/10	0.9	54.1	163.3	3.8	AMS <sup>a</sup>	Older boundary: cal. <b>18,862–18,636 (cal. 16,912–16,686 BC)</b>	13,950–12,920 (11,420–10,830) 10,190–9,870
Blandano lava flow (flow-mean made by site-mean) + ETN80 + ETN81	ETN77	3/3	8.3	55.5	319.5	6.9			8,670–8,650
Blandano lava flow (flow-mean made by ChRMs)	<b>27/30</b>	<b>7.9</b>	<b>55.2</b>	<b>129.4</b>	<b>2.5</b>	122 BC tephra layer	Younger boundary: <b>2,072 (122 BC)</b>	7,380–7,210 (5,700–5,460) 4,340–4,060	
Trecastagni lava flow	ETN58	9/10	20.5	72.1	72.6	6.1	Below Monte Serra flow		3,730–3,580 (3,580–3,440) (3,130–3,040)
	ETN59	9/10	16.6	69.3	115.8	4.8			
	ETN60	8/10	350.9	76.1	96.0	5.7			
Trecastagni lava flow (flow-mean made by site-mean)	ETN61	9/10	19.0	67.4	147.5	4.0		<sup>a</sup>	
Trecastagni lava flow (flow-mean made by site-mean) + ETN59 + ETN60 + ETN61	ETN58	4/4	13.5	71.5	216.2	6.3	$^{226}\text{Ra}/^{230}\text{Th}$ <sup>d</sup>	Older - Younger boundary: <b>8,700–4,080</b>	5,620–5,500
Trecastagni lava flow (flow-mean made by ChRMs)	<b>38/40</b>	<b>14.9</b>	<b>72.4</b>	<b>65.2</b>	<b>2.9</b>				<sup>a</sup>
Monte Serra lava flow	ETN56	10/10	12.2	55.0	82.6	5.3	Above Blandano flow		
	ETN78	10/10	7.1	45.5	94.7	5.0			

**Table 1**  
*Continued*

Volcanic unit	Site	n/N	D°	I°	k	$\alpha_{95}^{\circ}$	Method	Age constraint (yr BP)	Inferred age (yr BP)
Monte Serra lava flow (flow-mean made by site-mean)	ETN79	10/10	4.9	48.1	221.0	3.3	$^{226}\text{Ra}/^{230}\text{Th}$ (Trecastagni flow) <sup>d</sup>	Older boundary: <b>8,700</b> -4,080	(8,700-8,200) (7,370-6,830)
Monte Serra lava flow (flow-mean made by ChRMss)	ETN56 + ETN78 + ETN79	3/3	7.8	49.6	221.7	8.3	122 BC tephra layer	Younger boundary: <b>2,072</b> (122 BC)	(6,580-6,510) (6,110-6,070) 5,540-5,320
Monte Gorna lava flow (flow-mean made by ChRMss)	ETN82	10/10	348.5	51.2	79.6	5.4	$^{226}\text{Ra}/^{230}\text{Th}$ <sup>c</sup>	Older boundary: <b>3,470</b> -1,910	<sup>b</sup> Older boundary: <b>8,639</b> -8,163
Monte Gorna lava flow (flow-mean made by site-mean)	ETN83	10/10	6.7	65.6	91.4	5.1	$^{226}\text{Ra}/^{230}\text{Th}$ <sup>c</sup>	Older boundary: <b>3,470</b> -3,330	(7,370-6,830)
Monte Gorna lava flow (flow-mean made by site-mean)	ETN84	10/10	359.8	60.3	321.8	2.7	$^{226}\text{Ra}/^{230}\text{Th}$ <sup>c</sup>	Younger boundary: <b>2,072</b> (122 BC)	3,010-2,980 2,520-2,070
Pisano lava flow (flow-mean made by ChRMss)	ETN68	10/10	347.6	56.6	372.8	2.5	$^{14}\text{C}$ <sup>f</sup>	Older boundary: <b>8,639</b> -8,163	<sup>a</sup> (cal. <b>6,689</b> -6,213 BC)
Pisano lava flow (flow-mean made by site-mean)	ETN70	9/9	350.4	56.2	86.9	5.6	$^{14}\text{C}$ <sup>f</sup>	Younger boundary: <b>2,072</b> (122 BC)	8,120-7,440 (2,380-2,130)
Pisano lava flow (flow-mean made by ChRMss)	ETN68 + ETN70	2/2	349.0	56.4	5,127.5	3.5	122 BC tephra layer	Older boundary: <b>8,639</b> -8,163	<sup>a</sup> (cal. <b>6,689</b> -6,213 BC)
Passopomo lava flow (flow-mean made by site-mean)	ETN69	9/10	348.9	56.4	152.5	2.7	$^{14}\text{C}$ <sup>f</sup>	Older boundary: <b>8,639</b> -8,163	<sup>a</sup> (8,640-8,170)
Passopomo lava flow (flow-mean made by site-mean)	ETN74	9/10	5.9	51.0	157.5	4.1	$^{14}\text{C}$ <sup>f</sup>	Younger boundary: <b>2,072</b> (122 BC)	6,150-5,990
Passopomo lava flow (flow-mean made by site-mean)	ETN69 + ETN74	2/2	1.2	44.7	69.7	6.2	$^{14}\text{C}$ <sup>f</sup>	Older boundary: <b>8,639</b> -8,163	5,470-5,320
Passopomo lava flow (flow-mean made by ChRMss)	ETN69 + ETN74	3/4	3.4	47.9	264.9	15.4	122 BC tephra layer	Younger boundary: <b>2,072</b> (122 BC)	5,200-4,350
Mangano lava flow (flow-mean made by site-mean)	ETN71	10/10	3.4	47.9	85.2	3.8	$^{14}\text{C}$ <sup>f</sup>	Older boundary: <b>8,639</b> -8,163	4,160-3,600
Mangano lava flow (flow-mean made by site-mean)	ETN72	10/10	357.9	61.6	82.0	5.4	$^{14}\text{C}$ <sup>f</sup>	Older boundary: <b>8,639</b> -8,163	<sup>a</sup> (7,610-7,450)
Mangano lava flow (flow-mean made by site-mean)	ETN73	10/10	358.2	62.3	206.1	3.4	122 BC tephra layer	Younger boundary: <b>2,072</b> (122 BC)	5,690-5,470
Mangano lava flow (flow-mean made by site-mean)	ETN71 + ETN72 + ETN73	3/3	359.8	62.3	2,740.5	2.4	$^{14}\text{C}$ <sup>f</sup>	Younger boundary: <b>2,072</b> (122 BC)	3,170-3,120 (2,550-2,100)
		<b>30/30</b>	<b>359.7</b>	<b>62.3</b>	<b>138.6</b>	<b>2.2</b>			

**Table 1**  
*Continued*

Volcanic unit	Site	n/N	D°	I°	k	$\alpha_{95}^{\circ}$	Method	Age constraint (yr BP)	Inferred age (yr BP)
<b>Mangano lava flow (flow-mean made by ChRMss)</b>									
<b>Monte Arcimis lava flow</b>	ETN62	9/10	2.0	63.1	229.5	3.4	$^{14}\text{C}^{\text{f}}$	Older boundary: cal. <b>8,639–8,163</b> (cal. <b>6,689–6,213 BC</b> )	5,660–5,490
	ETN63	10/10	12.9	68.5	81.2	5.4		Younger boundary: <b>2,072</b> (122 BC)	3,390–3,150
	ETN64	10/10	351.8	68.7	109.2	4.6	122 BC tephra layer		2,770–2,620
Monte Arcimis lava flow (flow-mean made by site-mean)	ETN62 + ETN63 + ETN64	3/3	2.2	67.0	252.5	7.8			2,480–2,390
Monte Arcimis lava flow (flow-mean made by ChRMss)		<b>29/30</b>	<b>2.3</b>	<b>67.1</b>	<b>92.0</b>	<b>2.8</b>			
<b>Cancellieri lava flow</b>									
	ETN65	10/10	0.6	62.6	141.9	4.1	$^{14}\text{C}^{\text{f}}$	Older boundary: cal. <b>8,639–8,163</b> (cal. <b>6,689–6,213 BC</b> )	(8,120–7,430) 2,390–2,100
	ETN66	10/10	347.0	59.4	141.6	4.1			
	ETN67	10/10	345.8	56.3	148.0	4.0			
Cancellieri lava flow (flow-mean made by site-mean)	ETN65 + ETN66 + ETN67	3/3	350.7	59.6	248.0	7.8	122 BC tephra layer	Younger boundary: <b>2,072</b> (122 BC)	
Cancellieri lava flow (flow-mean made by ChRMss)		<b>30/30</b>	<b>350.7</b>	<b>59.6</b>	<b>108.2</b>	<b>2.5</b>			
<b>Dagala lava flow</b>									
	ETN75	8/10	357.0	55.8	44.7	8.4	$^{14}\text{C}^{\text{f}}$	Older boundary: cal. <b>8,639–8,163</b> (cal. <b>6,689–6,213 BC</b> )	8,160–7,340 5,770–5,630
	ETN76	8/10	350.0	61.3	114.8	5.2			
Dagala lava flow (flow-mean made by site-mean)	ETN75 + ETN76	2/2	353.8	58.6	302.1	14.4			5,510–5,430
Dagala lava flow (flow-mean made by ChRMss)		<b>16/20</b>	<b>353.7</b>	<b>58.6</b>	<b>61.6</b>	<b>4.7</b>	Paleomagnetic dating (Prinoti flow) <sup>g</sup>	Younger boundary: 1,300– <b>1,200</b>	4,960–4,900 4,560–4,530 4,360–4,310 3,490–3,370

Note. n/N indicates either number of characteristic remanent magnetization (ChRM) directions used to calculate the site mean direction/total number of cores drilled at a site or number of ChRMs used to calculate a volcanic unit mean direction/total number of samples from the volcanic unit. D and I are the mean paleomagnetic declinations and inclinations, respectively. k and  $\alpha_{95}$  are the precision parameter and the confidence limit, respectively, after Fisher (1953). Asterisks indicate the discarded sites. Inferred ages are gathered by comparing “flow-mean made by ChRMs” paleomagnetic directions (in bold) with (a) 14 ky global Palaeosecular Variation (PSV) model by Pavón-Carrasco et al. (2014), and (b) 4 ky regional PSV model by Pavón-Carrasco et al. (2021). Exceptions are the 19–14 ky BP (17–12 ky BC) intervals of Monte San Leo, Camporotondo Einco, and Blandano flows, indicating their possible age range beyond the PSV curve. The conversions of AMS (Accelerator Mass Spectrometry method, yr BP) and  $^{14}\text{C}$  (yr BP) conventional ages into calendar-calibrated ages (cal yr AD–BC) were obtained by means of INTCAL20 (Reimer et al., 2020) terrestrial radiocarbon age calibration with the Radiocarbon Calibration Program CALIB8.1.0 (Stuiver et al., 2021). All ages are reported with corresponding uncertainties at the 2σ level. Site references: <sup>a</sup>Coltellini et al. (2000), <sup>b</sup>Branca et al. (2021), <sup>c</sup>Tanguy et al. (2012), <sup>d</sup>Tanguy et al. (2007), <sup>e</sup>Magli et al. (2022), <sup>f</sup>Calvari and Groppelli (1996). <sup>g</sup>This work. Ages in bold are those used as younger/older bounds of the independent age windows (see Text S1 in Supporting Information S1 for details). Both age constraints and paleomagnetic ages are expressed in yr BP (before AD 1950) and yr BC–AD. Age constraints of the ninth column (expressed in yr BP) are obtained by adding/subtracting AD 1950 to the age constraints of column tenth (reported in yr BC–AD). Inferred ages by parenthesis are discarded by stratigraphic evidence (see the text for the discussion).

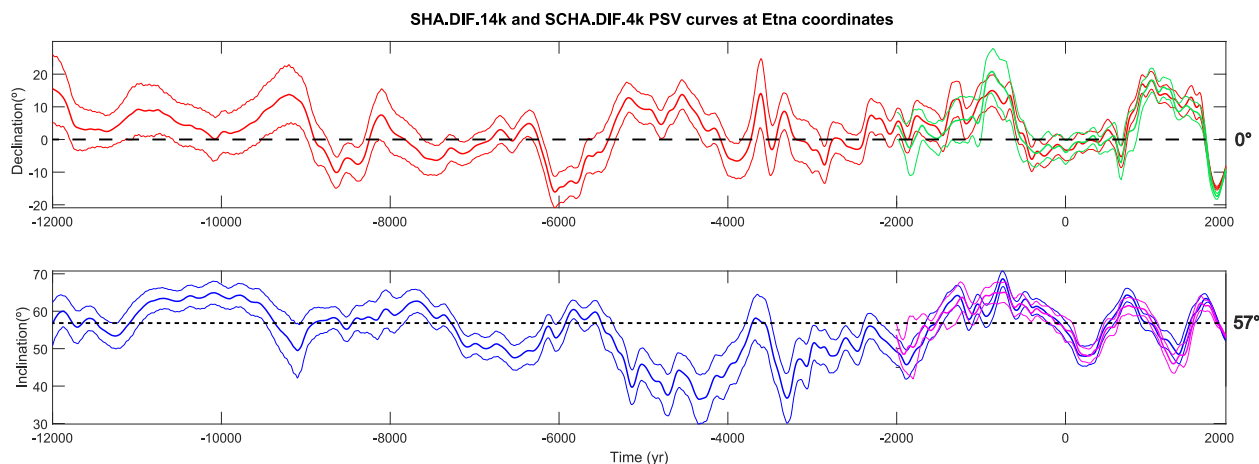


**Figure 3.** Comparison between SHA.DIF.14k (Pavón-Carrasco et al., 2014) and SCHA.DIF.4k (Pavón-Carrasco et al., 2021) models at Etna coordinates. The plots show the variation in declination (upper plot) and inclination (lower plot) over time. Bold and thin lines represent the Paleo-Secular Variation values and  $2\sigma$ -errors (red and blue lines for SHA.DIF.14k, green and purple lines for SCHA.DIF.4k). Dashed and dotted black lines indicate declination and inclination of the GAD field direction, respectively.

dating method may be achieved for European volcanoes, whereas its use is limited in remote world areas where PSV data are sparse (Carrancho et al., 2013; Kovacheva et al., 2014; Molina-Cardín et al., 2018; Pavón-Carrasco et al., 2014, 2021; Rivero-Montero, Gómez-Paccard, Carrasco, et al., 2021; Rivero-Montero, Gómez-Paccard, Kondopoulou, et al., 2021; Schanner et al., 2022; Speranza et al., 2008; Tema & Lanos, 2021). Thus, Etna is the perfect site to test the validity of paleomagnetic dating with best method pre-requisites, as here: (a) Etna volcano stratigraphy is very accurate thanks to several decades of investigation, (b) several radiometric and archeologic age constraints exist, and (c) the accuracy of the PSV reference model is very high, compared to other localities worldwide.

### 3.2. Accuracy of Paleomagnetic Dating

Paleomagnetic dating accuracy has been intensely debated over the past few decades, and many studies have tried to quantify the sources of bias affecting the geomagnetic field record in volcanics. In a pioneer study, Doell and Cox (1963) compared the paleomagnetic directions retrieved from nine Hawaiian historic lava flows of known age with the known direction of the geomagnetic field. They achieved geo-paleomagnetic direction coincidence within 0.2–3.8°, and found 3°–5° paleomagnetic direction 95% confidence cones from the same flow, comparable with values obtained during following decades at other worldwide volcanoes: Hawaii (Hagstrum & Champion, 1994; Holcomb et al., 1986), New Zealand (Greve et al., 2016; Robertson, 1986), Mexico (Böhnle et al., 2016; Juárez-Arriaga et al., 2018; Mahgoub, Böhnle, Siebe, & Chevrel, 2017; Mahgoub, Böhnle, Siebe, Salinas, & Guilbaud, 2017; Mahgoub et al., 2018), Germany (Böhnle & Schnepf, 1999); Chile (Roperch et al., 2015), and Italy (Vulcano: Lanza & Zanella, 2003; Stromboli: Quidelleur et al., 2005; Speranza et al., 2004, 2008; Etna: Rolph & Shaw, 1986; Speranza et al., 2006; Risica et al., 2019).

In recent years, Pinton et al. (2018) tested the method at higher latitudes (Iceland). In particular, for the Eldgjá (AD 934–938) and Laki (AD 1,783–1,784) lavas, paleomagnetic ages of AD 730–1,030 and AD 1,750–1,850, respectively, were obtained, both encompassing the known emplacement ages of the two eruptions.

For the great majority of the studies, sampling was carried out using the classical paleomagnetic technique of drilling 2.5 cm-diameter cores in the volcanics, orienting them in situ, and measuring the remanent magnetization by stepwise thermal or alternating field cleaning until complete demagnetization. Concerning dating accuracy, the classical paleomagnetic method, when applied to some Italian volcanoes (e.g., Etna, Vesuvius, Stromboli, and Vulcano), provided relatively small  $\alpha_{95}$  values (e.g., 2°–4° by Speranza et al., 2004, 2005; 3°–6° by Lanza & Zanella, 2003, p. 2.1°–2.5° by Zanella et al., 2000), translating into best dating accuracy of one-two centuries.

It must be acknowledged, however, that unfaithful paleomagnetic recording of the geomagnetic field has been reported in some cases (e.g., Brown & Mertzman, 1979; Castro & Brown, 1987; Lanza et al., 2005a; Urrutia-



**Figure 4.** Petrographic microscope (cross-polarized light) images of Blandano (a–c), Trecastagni (d–f), and Cancellieri (g–i) lava flows describing representative rock-mineral textures. Pl = plagioclase, Cpx = clinopyroxene, OI = olivine. (a–b and d–e): Porphyritic textures with abundance of plagioclase (a–b) and plagioclase, clinopyroxenes, and olivine (d–e) phenocrysts (4x magnification). (e): Evidence of globomerocrysts of Pl, Cpx, and OI. (g–h): Sub-aphyratic textures with scarce plagioclase, clinopyroxene, and olivine phenocrysts. (c, f and i): Details of groundmass (10x magnification): prevalent intersertal (c and f) and less common pilotaxitic (i) textures.

Fucugauchi et al., 2004). These discrepancies were inferred to depend upon several factors such as mineral magnetic variability within the volcanic unit, mechanical factors, and local deflections of the paleo-geomagnetic field due to the magnetization of the underlying terrain or the cooling flow itself (e.g., Lanza & Zanella, 2006; Speranza et al., 2006).

On Mount Etna, paleomagnetic dating accuracy was investigated on 13 historic (i.e., younger than 2,750 yr BP) lava flows by Speranza et al. (2006). They first proved method reliability by successfully dating four test flows with known age. Afterward, they paleomagnetically dated nine loosely dated lava flows, providing 136–661 years (average 307 years) age ranges. Thus, our work virtually represents the follow up of Speranza et al.'s (2006) work, extending the method test on pre-historic Holocene flows.

#### 4. Sampling and Methods

During May 2021, we sampled 44 paleomagnetic sites from 15 different lava flows, while another site (ETN100) was sampled from Monte Trigona flow in July 2023. The Monte San Leo, Monte Trigona, and Trecastagni lava flows have been investigated with four sampling sites; the Pisano, Passopomo and Dagala lava flows with two sampling sites; the remaining 10 lava flows have been investigated with three sampling sites each. Site locations are shown in Figure 2 and Table 1, and detailed in Text S1 and Table S1 in Supporting Information S1. Sampling sites have been carefully selected aiming at reaching the inner and unaltered flow parts, to avoid possible post-cooling tilt of the upper scoriaceous flow levels (Valet & Soler, 1999), and spacing them 20–50 m across available outcrops.

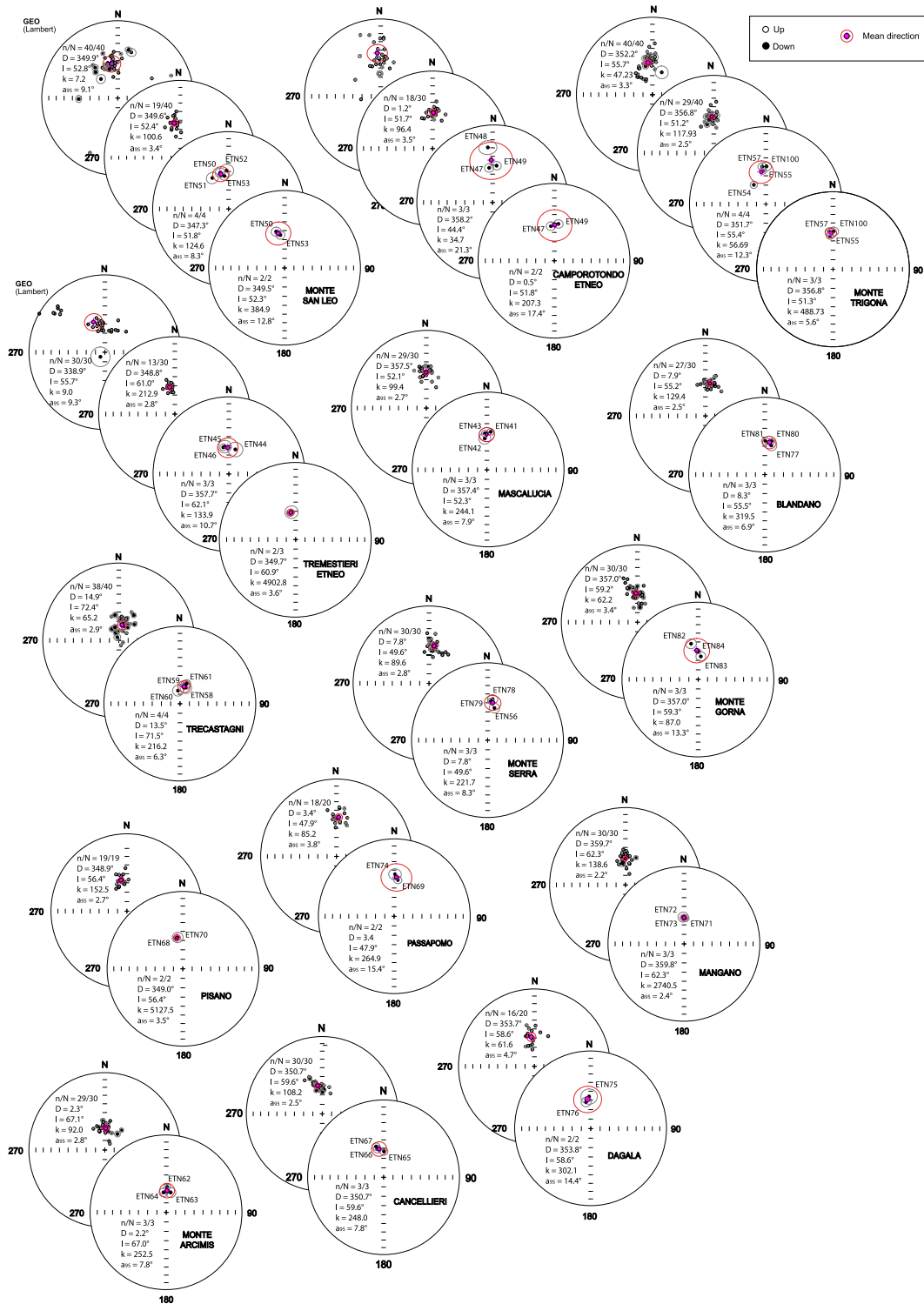


**Figure 5.** Equal-area projections (lower hemisphere) of mean paleomagnetic directions from the Mount Etna lava flows. For each studied eruption, two plots are displayed, showing the “flow-mean made by ChRMs” (plot behind) and “flow-mean made by site-means” (plot ahead) paleomagnetic directions. For Monte San Leo, Camporotondo Etneo, Tremestieri Etneo, and Monte Trigona lava flows, other two plots representing all the ChRMs from each sample and the “flow-mean made by site-means” paleomagnetic direction excluding discarded sites, respectively, are also displayed. Black points represent ChRMs in the “flow-mean made by ChRMs” plot, and site-mean paleomagnetic directions in the “flow-mean made by site-means” plot. Purple points represent the mean paleomagnetic directions (calculated either averaging ChRMs or site-mean directions), and the ellipses around the paleomagnetic directions are the projections of the relative  $\alpha_{95}$  cones. D, declination; I, inclination;  $\alpha_{95}$ , statistical parameter after Fisher (1953).

At each site, we drilled 10 2.5 cm diameter cores using a petrol-powered portable drill cooled by water, and oriented them in situ by both a magnetic and a sun compass, for a total number of 450 oriented cores. The local field declination values (i.e., the difference between the magnetic and sun compass readings) varied from 94.6° to –41° (average 1.3°), and are most comprised between 15° and –10°. The larger field declination values were likely due to lightning-induced isothermal remanent magnetization (IRM) that significantly deflected the compass needle.

All sampled cores were cut into standard 2 cm-long cylindrical specimens and their Natural Remanent Magnetization (NRM) was measured in the shielded room of the Renato Funiciello paleomagnetic laboratory at Istituto Nazionale di Geofisica e Vulcanologia (Rome), by a 2G Enterprises direct current super-conducting quantum interference device (SQUID) cryogenic magnetometer. For all specimens 10 progressive Alternating Field (AF) demagnetization steps, up to a maximum peak field of 120 mT, were selected.

AF demagnetization data were represented on orthogonal demagnetization diagrams (Zijderveld, 1967) and on equal-area projections, and the magnetization components were isolated by principal component analysis (Kirschvink, 1980). Site-mean and flow-mean paleomagnetic directions were computed using Fisher's (1953) statistics. “Site-mean” paleomagnetic directions were obtained by averaging characteristic remanent magnetization directions (ChRMs) from the same site. The flow-mean paleomagnetic directions were obtained by averaging either site-mean directions from the same lava flow (“flow-mean made by site-means”) or ChRMs from the same flow (“flow-mean made by ChRMs”), as the number of specimens from each site is the same. “Flow-mean made by ChRMs” paleomagnetic directions are obviously better defined (significantly smaller  $\alpha_{95}$  values) than those of “flow-mean made by site-means,” and were used for paleomagnetic dating in this work. Paleo-intensity values would have been obviously useful to obtain more refined paleomagnetic ages, but were not determined due to lack of paleo-intensity facilities at the Rome paleomagnetic laboratory.

Paleomagnetic dating was carried out by comparing the “flow-mean made by ChRMs” paleomagnetic directions with the SHA.DIF.14k PSV global model (covering the last 14 ky, Pavón-Carrasco et al., 2014) and—only for the Monte Gorna eruption, younger than 4 ka—with the SCHA.DIF.4k PSV regional model (covering the last 4 ky, Pavón-Carrasco et al., 2021; Figure 3). We chose the two models as they both take advantage of a high number of paleomagnetic data from archeological remains and volcanic products and exclude sedimentary data sets, thus avoiding bias due to data smoothing and possible sedimentary inclination shallowing (e.g., Speranza et al., 2008). Dating accuracy of the two PSV models decreases for ages older than few millennia due to the lower number of PSV reference data. In particular, the SHA.DIF.14k global model is well defined up to 6 ka BC, while for 6–12 ka BC the data set is much less robust (Schanner et al., 2022). On the other hand, the SCHA.DIF.4k model, given its higher reference data number between 2000 BC and 0, has a better accuracy than that of SHA.DIF.14k for such age window.

Paleomagnetic dating was performed using the “Archaeo\_dating” Matlab tool of Pavón-Carrasco et al. (2011), which first calculates the expected geomagnetic directions at the study area. Then, it compares them to paleomagnetic directions of volcanic units through a Bayesian statistical approach (Lanos, 2004), obtaining matching age interval(s) at 95% (or 65%) probability. The initial age windows of direction comparison relied on stratigraphic evidence and, when available, on radiometric datings, as well as on paleomagnetic age constraints from overlying/underlying lava flows (Table 1).

Further analyses were carried out to characterize the magnetic mineralogy of the investigated lava flows and to test whether sites from the same flow shared similar magnetic characteristics. In particular, for each sample, we calculated the Q Königsberger ratio (e.g., Kono, 2015), that is, the ratio between remanent (NRM) and induced magnetization intensities. The latter is the product of  $k$  (bulk volume susceptibility measured with a MFK1-Multifunction Kappabridge) and  $B$  (the Earth's magnetic field total intensity at Mount Etna 45,310 nT in May 2021 and 45,450 nT on July 2023, according to the IGRF model). On crushed powders from one specimen per each lava flow we also measured the variation of the low-field magnetic susceptibility during heating and cooling cycles performed in air, from room temperature up to 700°C, using an MFK1 Kappabridge coupled with a CS-3 furnace. The Curie temperature ( $T_c$ ) of the magnetic minerals was determined from the thermomagnetic curves as the temperature (or range of temperatures) at which paramagnetic behavior starts to dominate (Petrovský & Kapička, 2006).

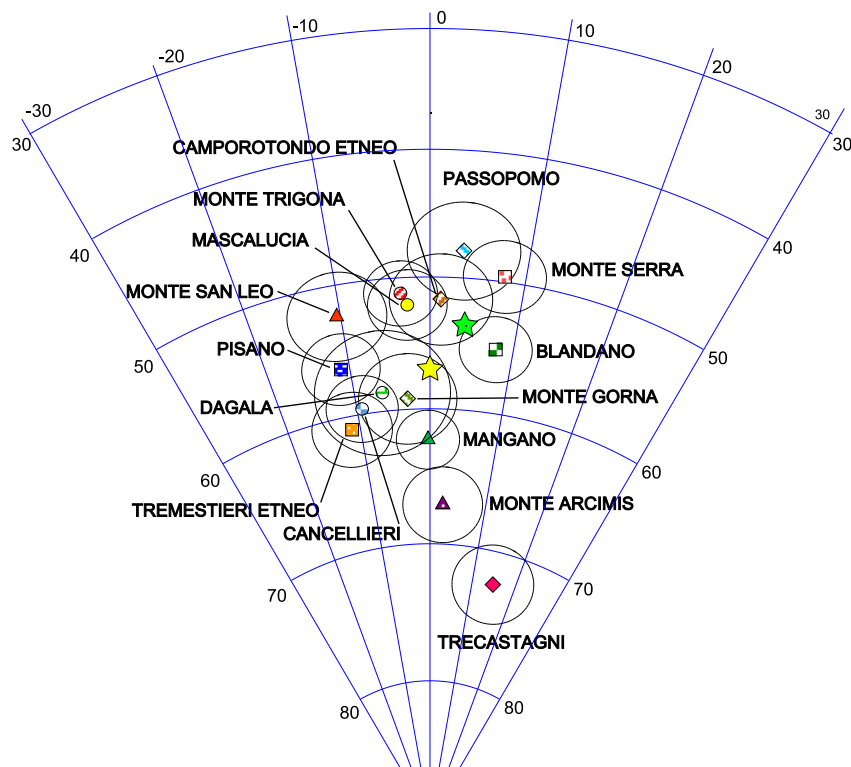


**Figure 6.** Equal-area projection (lower hemisphere) of “flow-mean made by ChRMs” paleomagnetic directions from the lower southeastern flank of Mount Etna volcano. The ellipses around the paleomagnetic directions are the projections of the related  $a_{95}$  cones. The yellow and green stars indicate the GAD field direction and the local geomagnetic field direction (IGRF model, May 2024), respectively. All paleomagnetic directions are listed in Table 1.

In addition to the paleomagnetic measurements, petrographic observations have been carried out on 45 thin sections of rock samples collected in each site. Modal analyses were carried out on high-resolution thin section scans (three random scans for each thin section; see Figures S2a–S2d in Supporting Information S1) by image analysis using the ImageJ software (Schneider et al., 2012). The vesicles and mineralogical phases (i.e., crystals >0.5 mm in diameter) were manually discriminated. The Porphyricity Index (P.I.) has been calculated and represents the total phenocrysts abundance expressed as volume %, vesicles-free (see Table S2 in Supporting Information S1).

## 5. Results

### 5.1. Petrographic Analyses

The petrographic analyses have been carried out aiming at verifying whether sites from the same flow effectively shared similar petrographic features. Our observations on the sampled lava flows show the most common mineralogical assemblage of Etna historical and prehistorical volcanics (Corsaro & Pompilio, 2004) which consists mainly of phenocrysts of plagioclase (Pl), with less abundant clinopyroxene (Cpx), olivine (Ol) and opaque oxide (Ox). Rocks show essentially a porphyritic texture, with large phenocrysts (1–7 mm) inside a hypocrystalline groundmass (Figure 4). The Porphyricity Index ranges between ca. 2–10 vol% for Blandano flow (Figure 4a–4c, and Table S2 in Supporting Information S1) and 30–40 vol% for Trecastagni flow (Figure 4d–4f, and Table S2 in Supporting Information S1), except for the Cancellieri (Figure 4g–4i) and Pisano flows that are aphyric. Plagioclase prevails over the other femic minerals (around 7–30 vol%, Figures S2e and S2f, and Table S2 in Supporting Information S1). Plagioclase crystals are euhedral and most of them are 2–5 mm in size (see Figure S2g in Supporting Information S1), with common larger (up to 5.5–7 mm) crystals, frequently showing complex zoning and sieve textures. Clinopyroxene (<7 vol%, Table S2 in Supporting Information S1) is generally idiomorphic. Phenocrysts range from 0.5 to 4 mm in size (Figure S2g in Supporting Information S1); the largest ones commonly show strong compositional zoning and enclose other minerals (essentially opaque oxides and

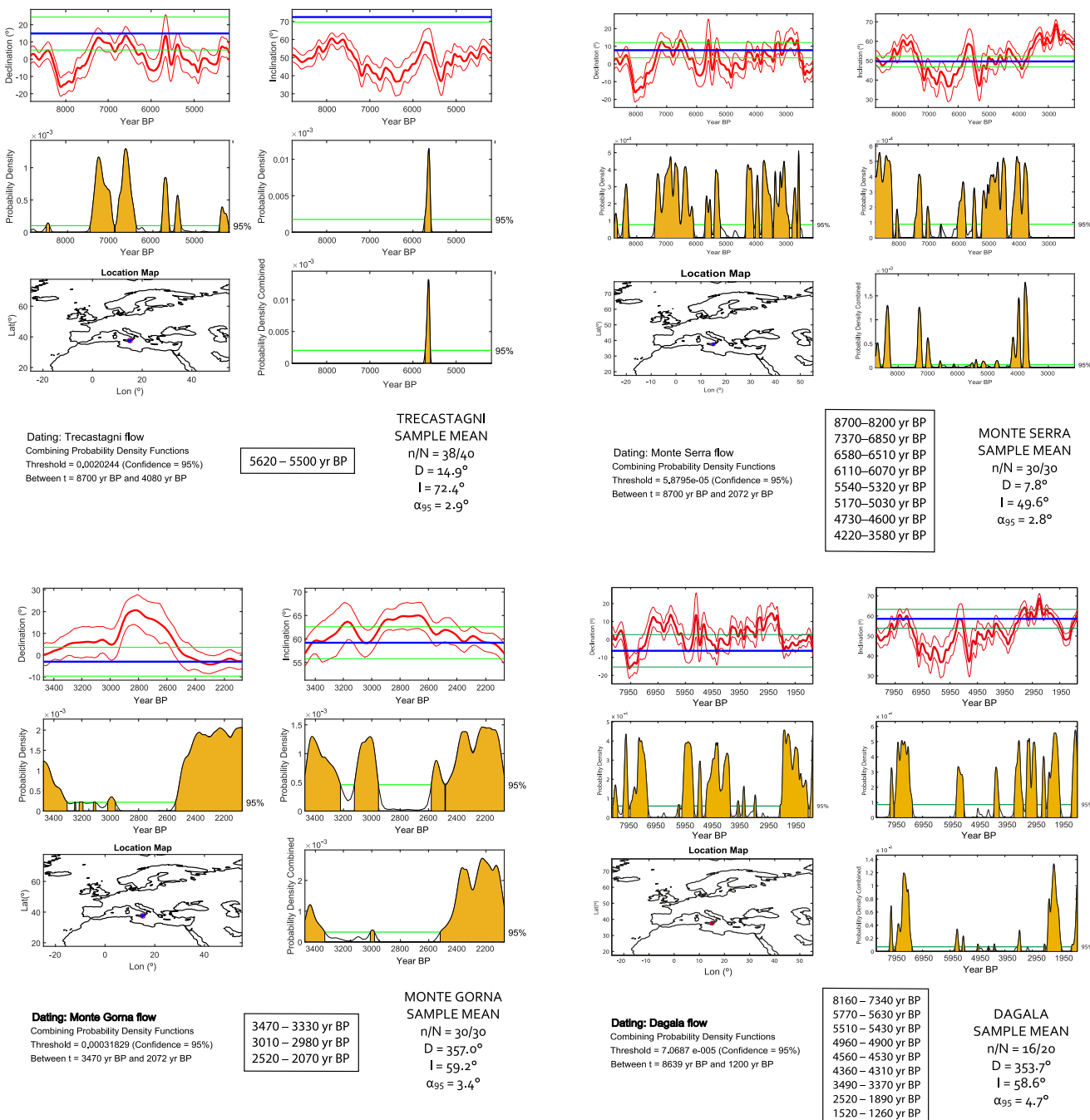


**Figure 7.** Paleomagnetic dating results of the Trecastagni, Monte Serra, Monte Gorna, and Dagala flows are shown according to the Pavón-Carrasco et al. (2011) method and software and the paleo-secular variation (PSV) reference models of Pavón-Carrasco et al. (2014; for Trecastagni, Monte Serra, and Dagala) and Pavón-Carrasco et al. (2021; for Monte Gorna). The left-hand panel shows the PSV curves (red lines) for the declination and the right-hand panel for the inclination (thin red lines for the associated errors, 95% confidence level), along with the probability density curves (in orange-shade). Paleomagnetic declination and inclination values are shown in blue straight lines; the 95% associated errors are in green straight lines. In the probability density graphs, the 95% confidence level is shown as a green line. Ages are in yr BP (before AD 1950).

subordinate plagioclase and olivine). Olivine ( $\leq 3$  vol%, 0.5–2.5 mm in size; Figures S2e–S2g and Table S2 in Supporting Information S1) is generally rounded and locally shows evidence of iddingsitic alteration. Glomeroporphyritic aggregates formed by plagioclase and/or mafic minerals (clinopyroxene and/or olivine) are quite common and reach several millimeters in size (Figure 4e).

The same minerals described above form the groundmass (ca. 60%–90% of the total volume, except for the aphyric Cancellieri and Pisano flows; Table S2 in Supporting Information S1) which mostly shows an inter-sertal texture, with microlites of clinopyroxene, olivine and opaque oxides entrapped in a network of plagioclase laths (Figures 4c and 4f). Pilotaxitic textures with iso-oriented plagioclase microlites (Figure 4i) are less common.

In summary, the petrographic analyses confirm that the lava units sampled for paleomagnetic dating actually correspond to those mapped in Branca, Coltelli, Groppelli, et al. (2011) and that each sampling site is therefore suited for the paleomagnetic investigation.

### 5.2. Magnetic Properties

The susceptibility versus temperature curves (or k-T curves, Figure S3 in Supporting Information S1) show a mostly irreversible variation trend in the heating-cooling cycles for about half of samples, with a substantial drop of magnetic susceptibility after cooling. About 80% of the samples display Curie temperatures ( $T_c$ ) between 500°C and 580°C, typical of magnetite or low Ti titano-magnetite; ~60% of the samples also show an inflection at 100–200°C and/or 350–450°C temperature ranges, consistent with the presence of titanomagnetite with intermediate to high Ti content.

NRM values of the samples range between 2.1 and 153 A/m (average 17 A/m), and their magnetic susceptibilities range between  $8.4 \times 10^{-4}$  and  $8.4 \times 10^{-2}$  SI (average  $3.5 \times 10^{-2}$ , Figure S4 in Supporting Information S1). Most of the highest NRM values are likely due to IRM induced by lightning strikes. Samples show Königsberger ratios between 3 and 182, mainly clustered between 5 and 50 Q slope lines (Figure S4 in Supporting Information S1), confirming the predominance of remanent over induced magnetization. As a rule, samples from the same lava flow show similar NRM and  $k$  values, although some of the studied eruptions (e.g., Monte San Leo) yield highly scattered values depending on either mineral magnetic variation (different  $k$  values) or lightning-induced IRM (different NRM but similar  $k$  values).

### 5.3. Paleomagnetic Directions

Apart for a viscous component eliminated at a peak AF of 20 mT, a well-defined ChRM was isolated for all samples in the 30–120 mT interval (Figures S5 and S6 in Supporting Information S1). Low magnetic coercivities are generally observed: ca. 90% of the samples demagnetized to <90% of the NRM, between 70 and 100 mT. About 10% of the samples (mostly from sites ETN47 of Camporotondo Etneo, ETN50 of Monte San Leo, ETN70 of Pisano, ETN76 of Dagala, and ETN84 of Monte Gorna) showed both low and high coercivities (only 70%–80% of the NRM was removed at the 120 mT AF peak field, see specimens ETN4701, ETN5008, and ETN8404 in Figure S5 and S6 in Supporting Information S1). However, thermomagnetic curves from the same specimens evidenced only magnetite and Ti-magnetite occurrence (Figure S3 in Supporting Information S1). The puzzling high-coercivity minerals with Curie temperatures <600°C observed in the 10% of the samples (consistent with previous evidence from basalts from Etna and other volcanoes: Branca et al., 2019; Magli et al., 2022; Risica et al., 2019, 2020; Speranza et al., 2006, 2008) are possibly related to single domain and/or deuterically oxidized Ti-magnetite (e.g., Dunlop & Özdemir, 2001).

In Figure 5, mean directions for each lava flow obtained averaging individual ChRMs and site-mean directions from each flow are shown. Flow-mean declinations (Table 1 and Figure 6) vary from 348.8° (Tremestieri Etneo) to 14.9° (Trecastagni), while inclinations fall between 47.9° (Passopomo) and 72.4° (Trecastagni). “Flow-mean made by ChRMs” paleomagnetic directions yield  $\alpha_{95}$  values between 2.2° and 4.7° (Mangano and Dagala flows, respectively), 3.0° on average (Table 1 and Figure 6), comparable with the 3°–5° values generally observed in lava flows (Doell & Cox, 1963; Lanza et al., 2005b).

Correlation of paleomagnetic directions from different sampling sites was frequently used in the past to assess if they belong (or not) to the same lava flow (or ignimbrite deposit, e.g., Di Chiara et al., 2012, 2014; Hagstrum & Champion, 1994; Pinton et al., 2018; Speranza et al., 2008, 2012; Zanella et al., 2001). Due to several paleomagnetic and volcano-tectonic reasons, the confidence cones of sites coming from the same volcanic unit do not always overlap (see discussion in Lanza & Zanella, 2006; Speranza et al., 2006, and evidence shown by Baag et al., 1995; Böhnle & Schnepf, 1999; Böhnle et al., 2009; Di Chiara et al., 2012; Knudsen et al., 2003; Pinton et al., 2018; Speranza et al., 2012; Tanguy & Le Goff, 2004; Valet & Soler, 1999). However, recent works (Branca

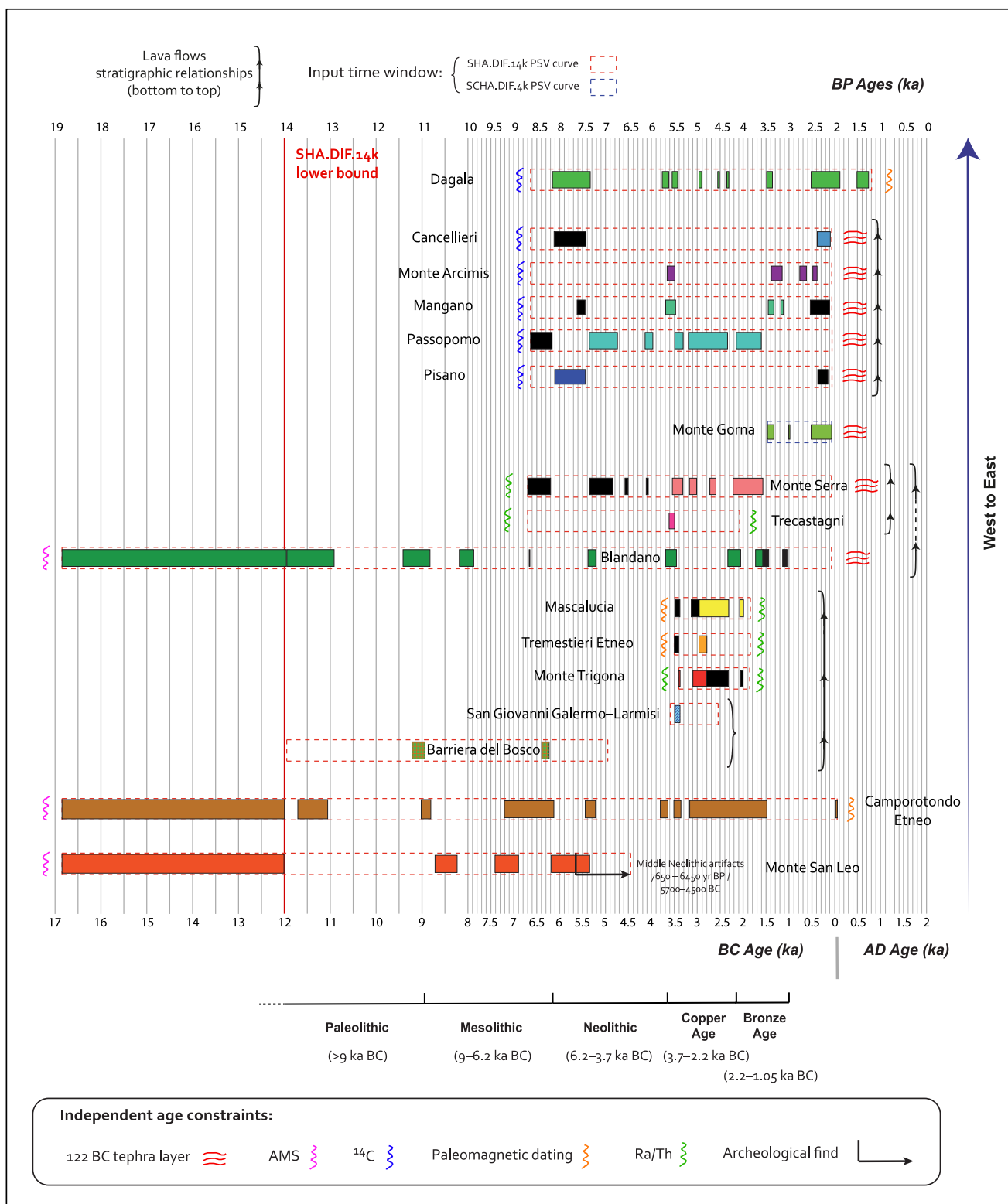


**Figure 8.**

et al., 2019; Malaguti et al., 2022; Pinton et al., 2018; Risica et al., 2019) showed that an angular distance of 10° between paleomagnetic directions from two sites can be used as threshold value (with a 95% probability) to assess whether they belong or not to the same volcanic unit. Our data basically confirm such criterion, as considering the whole paleomagnetic data set (thus sites undoubtedly coming from the same lava flow unit), inter-site angular distances are comprised in the 0.7°–12.2° range (except for the 17.1° angular distance between site-mean directions ETN82 and ETN83 of the Monte Gorna flow), and the 95% percentile corresponds to a 11.3° value (Figure S7 in Supporting Information S1). Following these considerations, site ETN54 was discarded, as its direction is >10° far from those of other sites from the same lava flow (Figure 5 and Table 1), thus it could belong to a different flow or to a tilted outcrop (i.e., the site is close to a fault; see Figure 2). Moreover, sites ETN44, ETN48, ETN51, and ETN52 were also excluded as characterized by high ChRM scatter ( $\alpha_{95} > 9^\circ$ ; Table 1), likely due to lightning-induced IRM affecting NRM (see Section 5.2). Furthermore, our paleomagnetic directions from Monte Serra and Monte Gorna flows are consistent with those obtained for the same eruptions by Tanguy et al. (2007) (angular distances <10°). Finally, the small (4.3°–6.1°) angular distances between site ETN100 and the other sites of Monte Trigona eruption (Figure S7 in Supporting Information S1) allow to definitively correlate the Monte Trigona scoria cone with the nearby lava flow.

#### 5.4. Paleomagnetic Dating

One or multiple paleomagnetic ages were obtained for each lava flow. Consecutive age spans were combined into a single age span when separated from each other by a time interval narrower than the precision of the PSV curve for that period: 75–100 years for the 4000 BC–AD 1900 time interval, 100–200 years for the 6000–4000 BC period, and 200–300 years for the 12,000–6000 BC time span (Pavón-Carrasco et al., 2014, 2021). Moreover, for three eruptions (Monte San Leo, Camporotondo Etneo, and Blandano), their common older boundary age (i.e., 18,862–18,636 yr BP) is ca. 5 ky older than the lower bound of the SHA.DIF.14k PSV curve (i.e., 14,000 yr BP), thus we paleomagnetically dated them, not excluding an age even older than 14 ka. Hopefully, the paleomagnetic directions from such flows will be useful for future paleomagnetic dating works, once additional constraints (i.e., new geologic/geochronological evidence and/or updated PSV models) will be available.

Three possible ages between 10,720 yr BP and 7,350 yr BP were found for the Monte San Leo eruption, along with 18,862–13,950 yr BP ages exceeding the 14 ka BP SHA.DIF.14k lower bound age (Table 1 and Table S1 in Supporting Information S1). Similarly, the Camporotondo Etneo lava flow yielded multiple probable age intervals between 13,710 yr BP and 1,950 yr BP, together with the 18,862–13,950 yr BP age window (Table 1 and Table S1 in Supporting Information S1).

Dating of the Mascalucia, Tremestieri Etneo, and Monte Trigona flows provided several matching age intervals, but some were discarded based on lava flows stratigraphic relationships described in Text S1 in Supporting Information S1, thus the following age spans are only considered: Monte Trigona 5,410–5,390 yr BP and 5,130–4,790 yr BP; Tremestieri Etneo 4,970–4,790 yr BP; Mascalucia 4,970–4,320 yr BP and 4,090–3,990 yr BP.

A single narrow age window (5,620–5,500 yr BP) was obtained for the Trecastagni flow (Figure 7). We assumed this age as the older boundary age for the overlying Monte Serra lava flow, thus obtaining for it four ages between 5,540 yr BP and 3,570 yr BP. Similarly, the Blandano lava flow yielded several paleomagnetic ages between 13,950 yr BP and 3,040 yr BP (discarding those younger than 3,580 yr BP, i.e., the upper bound of the youngest age span of the overlying Monte Serra flow), in addition to the 18,862–13,950 yr BP age interval (Table 1 and Table S1 in Supporting Information S1).

Concerning the group of Pisano, Passopomo, Mangano, Monte Arcimis, and Cancellieri, eruptions, several age intervals were obtained for each of them (Table 1 and Table S1 in Supporting Information S1). Taking into account the stratigraphic positions of the lava flows, some ages were excluded. In particular, the presence of a

**Figure 8.** Synthetic framework of the paleomagnetically inferred ages for the studied lava flows of the Etna southeastern slopes (discarded age intervals are in black; see text for details), along with the lava flows paleomagnetically dated by Magli et al. (2022). Dashed red and blue boxes indicate the lava flows' independent age constraints by dating through the SHA.DIF.14k and (only for Monte Gorna) SCHA.DIF.4k PSV reference curves, respectively. Older and younger independent age constraints of each lava flow are also reported. Vertical black arrows represent the stratigraphic relationships of lava flows stacks (from bottom to top). Ages are in yr BP (present is AD 1950) and yr BC–AD. The archeological phases of the Sicilian prehistory are also reported.

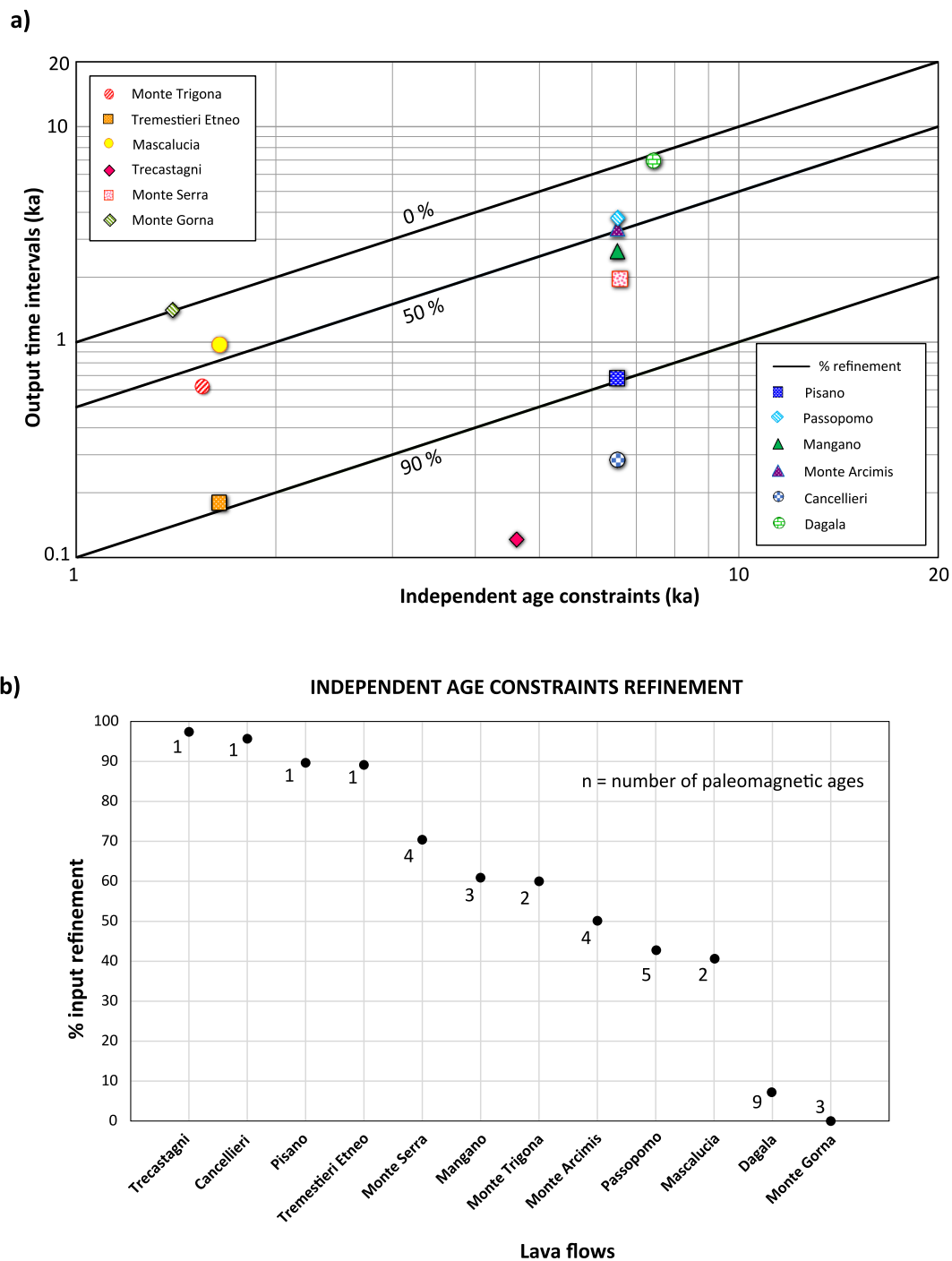


**Figure 9.** Graphs showing the initial age constraints refinement of the studied prehistoric flank eruption from Etna volcano. (a): independent age constraints (ka) versus output time intervals (ka) diagram, with the black sloping lines representing the initial ages refining of 0%, 50%, and 90%. (b): % values of initial age refinement for all the lava flows, with the number of paleomagnetic ages reported for each eruption.

paleosol (8,640–8,160 yr BP  $^{14}\text{C}$  age by Calvari & Groppelli, 1996) at the base of the Chiancone Member fluvial beds succession underlying the lava flows stack allows us to rule out the oldest age intervals of Cancellieri (8,120–7,430 yr BP) and Passopomo (8,640–8,170 yr BP) flows, which are temporally too close to enable the deposition of the sedimentary sequence. To sum up, the paleomagnetic ages obtained for each eruption of this group are: Pisano, a single 8,120–7,440 yr BP age; Passopomo, five age intervals between 7,360 yr BP and 3,600 yr BP;

**Table 2**

*Refinement of Age Control of the Prehistoric Flank Eruptions From the Mount Etna Southeastern Lower Slopes*

Lava flows	Overall paleomagnetic age intervals						Independent age constraints refinement (%)	Number of possible ages intervals in overall window	Stratigraphic notes
	Independent age constraints			Older bound (yr BP)	Younger bound (yr BP)	Total duration (yr)			
	Older boundary age (yr BP)	Younger boundary age (yr BP)	Total duration (yr)	Older bound (yr BP)	Younger bound (yr BP)	Total duration (yr)			
Monte Trigona	5,410	3,860	1,550	5,410	4,790	620	60.0	2	
Tremestieri Etneo	5,494	3,850	1,644	4,969	4,790	179	89.1	1	above Monte Trigona
Mascalucia	5,494	3,850	1,644	4,968	3,992	976	40.6	2	above Tremestieri Etneo
Trecastagni	8,700	4,080	4,620	5,616	5,495	121	97.4	1	below Monte Serra
Monte Serra	8,700	2,072	6,628	5,538	3,575	1,963	70.4	4	above Trecastagni and Blandano
Monte Gorna	3,470	2,072	1,398	3,470	2,072	1,398	0.0	3	
Pisano	8,639	2,072	6,567	8,115	7,436	679	89.7	1	
Passopomo	8,639	2,072	6,567	7,362	3,603	3,759	42.8	5	above Pisano
Mangano	8,639	2,072	6,567	5,687	3,118	2,569	60.9	3	above Passopomo
Monte Arcimis	8,639	2,072	6,567	5,658	2,390	3,268	50.2	4	above Mangano and Passopomo
Cancellieri	8,639	2,072	6,567	2,384	2,101	283	95.7	1	above Monte Arcimis and Mangano
Dagala	8,639	1,200	7,439	8,159	1,255	6,904	7.2	9	

*Note.* Older and younger boundary ages of independent age constraints and paleomagnetic ages intervals are expressed in yr BP (present is AD 1950).

Mangano, three possible age intervals of 5,690–5,470 yr BP, 3,450–3,330 yr BP, and 3,170–3,120 yr BP; Monte Arcimis, four equally possible ages between 5,660 yr BP and 2,390 yr BP; Cancellieri, a single 2,380–2,100 yr BP age.

Finally, multiple possible age spans between 8,160 yr BP and 1,260 yr BP were found for the Dagala eruption.

## 6. Discussion

A significant refinement of the chronology of 12 prehistoric Mount Etna flank eruptions was obtained in this work (Figure 8).

Our results first show that paleomagnetic ages were obtained for all the studied eruptions, even for those characterized by narrow (down to 1,398–1,644 years, Monte Gorna, Mascalucia, and Tremestieri Etneo) independent age constraints (Figure 8). This consistency is significant, as it shows that (a) the obtained paleomagnetic directions represent rather faithful proxies for geomagnetic field directions at the time of lava emplacement and cooling, and (b) that the same field directions are correctly provided by PSV models of Pavón-Carrasco et al. (2014, 2021). In particular, a comparison between paleomagnetic dating of Monte Gorna eruption by using the SCHA.DIF.4k (Figure 7) and SHA.DIF.14k (Figure S8 in Supporting Information S1) PSV models, shows similar paleomagnetic ages (differences of a few decades up to a century), thus proving models' consistency.

Second, a significant eruption age refinement has been obtained as paleomagnetic age spans are invariably shorter than the initial age constraints (Figure 9 and Table 2). Indeed, except for two lava flows (Monte Gorna and Dagala) whose initial age intervals (1,398–7,439 years) were poorly reduced by paleomagnetic dating (refinement of 0.0%–7.2%, 1,398–6,904 years), the other 10 eruptions yielded at least ca. 40% refinement (Figure 9 and Table 2). In particular, independent age constraints of six volcanic units (1,550–6,628 years) were reduced by 40% (Mascalucia, 980 years) to 70% (Monte Serra, 1,960 years), while four lava flows (Trecastagni, Cancellieri, Pisano, and Tremestieri Etneo) yielded a remarkable reduction of their initial time uncertainties

(1,644–6,567 years) up to 89.1%–97.4% (120–680 years; Figure 9 and Table 2). Well defined ages were obtained for about 30% of the flow characterized by long (>1.5 kyrs) independent age constraints. Two main groups of lava flows can be approximately distinguished (Figure 9a): (a) eruptions whose <7 kyrs long-initial age intervals generally gained an improvement higher than 40%–50%; (b) lavas bracketed in initial age constraints >7 kyrs which did not obtain a significant refinement after paleomagnetic dating. It must be noted though that even in group (c) paleomagnetic dating, while not conclusive, allows to exclude most the initial age constraints, so that future stratigraphic evidence could take advantage of paleomagnetic ages. An exception is the Monte Gorna eruption, whose narrow (1,398 years) independent time range obtained a null refining (Figure 9a).

In general, a single and very short age range (e.g., 120 years, Trecastagni eruption; Table 2) is found for lava flows recording “unusual” (high/low inclination/declination values) geomagnetic directions. Conversely, several age ranges (up to nine age spans with a mean interval of 243 years, Dagala eruption, Table 2) are obtained for lava flows recording paleomagnetic directions frequently reoccupied during the Holocene (Figure 3). Concerning lava flows stacks (e.g., the group of Pisano, Passopomo, Mangano, Monte Arcimis, and Cancellieri), some of the paleomagnetic ages could be discarded by considering stratigraphic relationships (Figure S9 in Supporting Information S1), thus allowing an age refining that would have been impossible to obtain for isolated and less constrained lava flows (e.g., Dagala; Figure S9 in Supporting Information S1). However, regardless of the number and length of the paleomagnetic ages obtained, paleomagnetism should be considered as an “incremental” method waiting for additional constraints (i.e., new stratigraphic, geochronological, and archeological evidence, as well as updated PSV models). Obviously, the combined use of paleomagnetism along with different dating methods is highly advisable to obtain reliable and accurate ages of Holocene volcanic rocks.

The new ages obtained may represent a starting point for assessing the frequency of the Holocene flank eruptions that opened vents below 1,000 m asl on SE Etna. By considering five of our prehistoric lava flows (Monte Gorna, Monte Trigona, Monte Serra, Trecastagni, and Pisano) and seven historic flank eruptions (AD 1669, AD 1329, Montarello, Monti Arsi di Santa Maria, Monte Ilice, Monpeloso, and Mompilieri; Figure S10 in Supporting Information S1), we get an almost homogeneous temporal distribution of lateral eruptions in the last ca. 5,500 years (i.e., about one event per five centuries). Exceptions are three lava flows (Montarello, Monti Arsi di Santa Maria, and Monte Ilice) clustered between 660 yr BP and 960 yr BP (Figure S10 and Table S3 in Supporting Information S1).

## 7. Concluding Remarks

Paleomagnetic dating of 12 mid-lower Holocene lava flows sampled in 45 different sites on the SE rift of Mount Etna (i.e., at a site where best method pre-requisites are verified), reveals that:

- Age solutions obtained at four flows characterized by narrow (1,398–1,644 yrs) independent age constraints suggest that both (a) paleomagnetism correctly yielded the geomagnetic field direction at the time of the lava emplacement and cooling, and (b) that reference PSV models used (Pavón-Carrasco et al., 2014, 2021) are reliable.
- At least a 40% refinement of initial age windows was obtained for 10 eruptions, and among them a ca. 90% refinement was obtained for four lava flows.
- When independent age intervals >1.5 kyrs are available, paleomagnetism is expected to provide successful dating for about 30% of the studied flows.
- Paleomagnetic ages reduce by more than 40%–50% the initial age intervals that are narrower than a 7,000 years-threshold value.
- Paleomagnetic dating allows to better refine ages of lava flows stacks with known stratigraphic relationships, than those of isolated and less constrained flows.
- When large (several millennia) independent age constraints are used and multiple age solutions are obtained, paleomagnetism should be regarded as an “incremental” method that could benefit from additional constraints in the future (i.e., new chrono-stratigraphic evidence and updated geomagnetic field models).
- A rather constant frequency (one lateral eruption every 500 years) seems to characterize the last 5,500 years eruptive history of SE Etna, the most urbanized (ca. 750,000 inhabitants) among Etna’s slopes.

## Conflict of Interest

The authors declare no conflicts of interest relevant to this study.

## Data Availability Statement

Paleomagnetic and petrographic data used for supporting this study are available at (Magli et al., 2023) with free access. Remasoft 3.0 and Cureval 8.0.2 softwares used for analyzing AF demagnetization data and thermomagnetic curves, respectively, are preserved at (Chadima, 2006; Chadima & Hrouda, 2012), available via free access. The “Archaeo\_Dating 8.0” Matlab tool used to carry out paleomagnetic dating is available at (Pavón-Carrasco et al., 2011) with free access. ImageJ 1.52t software used to calculate the abundance (volume %) of vesicles and mineralogical phases is preserved at (Schneider et al., 2012), available with free access. The CALIB8.1.0 program used to recalibrate radiocarbon ages to BC/AD is available at (Stuiver et al., 2021) with free access. Microsoft Office 365 (Excel and Power Point) and Adobe Illustrator CC 2017 have been used to create the graphs of petrographic analyses and ages refinement, and to edit the figures of this paper, respectively.

## Acknowledgments

This work is part of the AM PhD project. The owners of the Palmento Museum, the Terra Costantino winery, and the SAI Mascalucia cooperative are deeply thanked for having allowed our sampling in their properties. Alessandro Todrani is acknowledged for his help with the use of SCHA.DIF.4k model. We thank Federico Rossetti for allowing the use of his optical microscope for petrographic analyses. We are grateful to two referees (Harald Böhnel and an anonymous referee), to *JGR Solid Earth* Associate Editor Daniel Pastor-Galán, and to Editor Mark Dekkers for providing constructive comments on our manuscript that helped to improve the work considerably.

## References

- Ali, M., Oda, H., Hayashida, A., Takemura, K., & Torii, M. (1999). Holocene palaeomagnetic secular variation at Lake Biwa, central Japan. *Geophysical Journal International*, 136(1), 218–228. <https://doi.org/10.1046/j.1365-246X.1999.00718.x>
- Andronico, D., Cannata, A., Di Grazia, G., & Ferrari, F. (2021). The 1986–2021 paroxysmal episodes at the summit craters of Mt. Etna: Insights into volcano dynamics and hazard. *Earth-Science Reviews*, 220, 103686. <https://doi.org/10.1016/j.earscirev.2021.103686>
- Azzaro, R., Branca, S., Gwinnier, K., & Coltellini, M. (2012). The volcano-Tectonic map of Etna volcano, 1: 100.000 scale: An integrated approach based on a morphotectonic analysis from high-resolution DEM constrained by geologic, active faulting and seismotectonic data. *Italian Journal of Geosciences*, 131(1), 153–170. <https://doi.org/10.3301/IJG.2011.29>
- Baag, C., Helsley, C. E., Xu, S. Z., & Lienert, B. R. (1995). Deflection of paleomagnetic directions due to magnetization of the underlying terrain. *Journal of Geophysical Research*, 100(B6), 10013–10027. <https://doi.org/10.1029/95JB00148>
- Barrière, J., d’Oreye, N., Smets, B., Oth, A., Delhayé, L., Subira, J., et al. (2022). Intra-crater eruption dynamics at Nyiragongo (DR Congo), 2002–2021. *Journal of Geophysical Research: Solid Earth*, 127(4), e2021JB023858. <https://doi.org/10.1029/2021JB023858>
- Becerril, L., Larrea, P., Salinas, S., Mossoux, S., Ferrés, D., Widom, E., et al. (2021). The historical case of Paricutín volcano (Michoacán, México): Challenges of simulating lava flows on a gentle slope during a long-lasting eruption. *Natural Hazards*, 107(1), 809–829. <https://doi.org/10.1007/s11069-021-04607-x>
- Behncke, B., Neri, M., & Nagay, A. (2005). Lava flow hazard at Mount Etna (Italy): New data from a GIS-based study. In M. Manga & G. Ventura (Eds.), *Kinematics and dynamics of lava flows: Geological society of America special paper* (Vol. 396, pp. 189–208). <https://doi.org/10.1130/0-8137-2396-5.189>
- Biass, S., Bonadonna, C., Di Traglia, F., Pistolesi, M., Rosi, M., & Lestuzzi, P. (2016). Probabilistic evaluation of the physical impact of future tephra fallout events for the Island of Vulcano, Italy. *Bulletin of Volcanology*, 78(5), 1–22. <https://doi.org/10.1007/s00445-016-1028-1>
- Böhnel, H., Michalk, D., Nowaczyk, N., & Naranjo, G. G. (2009). The use of mini-samples in palaeomagnetism. *Geophysical Journal International*, 179(1), 35–42. <https://doi.org/10.1111/j.1365-246X.2009.04260.x>
- Böhnel, H., Pavón-Carrasco, F. J., Sieron, K., & Mahgoub, A. N. (2016). Palaeomagnetic dating of two recent lava flows from Ceboruco volcano, western Mexico. *Geophysical Supplements to the Monthly Notices of the Royal Astronomical Society*, 207(2), 1203–1215. <https://doi.org/10.1093/gji/ggw310>
- Böhnel, H., & Schnepp, E. (1999). Precision of the paleomagnetic method: An example from the Quaternary Eifel volcanics (Germany). *Earth Planets and Space*, 51(6), 403–412. <https://doi.org/10.1186/BF03352244>
- Bonadonna, C., Pistolesi, M., Biass, S., Voloschina, M., Romero, J., Coppola, D., et al. (2022). Physical characterization of long-lasting hybrid eruptions: The 2021 tajogaite eruption of cumbre vieja (La Palma, Canary Islands). *Journal of Geophysical Research: Solid Earth*, 127(11), e2022JB025302. <https://doi.org/10.1029/2022JB025302>
- Branca, S., & Abate, T. (2019). Current knowledge of Etna’s flank eruptions (Italy) occurring over the past 2500 years. From the iconographies of the XVII century to modern geological cartography. *Journal of Volcanology and Geothermal Research*, 385, 159–178. <https://doi.org/10.1016/j.jvolgeores.2017.11.004>
- Branca, S., Azzaro, R., De Beni, E., Chester, D., & Duncan, A. (2015). Impacts of the 1669 eruption and the 1693 earthquakes on the Etna Region (Eastern Sicily, Italy): An example of recovery and response of a small area to extreme events. *Journal of Volcanology and Geothermal Research*, 303, 25–40. <https://doi.org/10.1016/j.jvolgeores.2015.07.020>
- Branca, S., Caracciolo, F. D. A., Malaguti, A. B., & Speranza, F. (2019). Constraining age and volume of lava flow invasions of the Alcantara valley, Etna volcano (Italy). New insights from paleomagnetic dating and 3D magnetic modeling. *Journal of Volcanology and Geothermal Research*, 374, 13–25. <https://doi.org/10.1016/j.jvolgeores.2019.02.009>
- Branca, S., Coltellini, M., & GropPELLI, G. (2011). Geological evolution of a complex basaltic stratovolcano: Mount Etna, Italy. *Italian Journal of Geosciences*, 130(3), 306–317. <https://doi.org/10.3301/IJG.2011.13>
- Branca, S., Coltellini, M., GropPELLI, G., & Lentini, F. (2011). Geological map of Etna volcano, 1: 50,000 scale. *Italian Journal of Geosciences*, 130(3), 265–291. <https://doi.org/10.3301/IJG.2011.15>
- Branca, S., Condomines, M., & Tanguy, J. C. (2015). Flank eruptions of Mt Etna during the Greek–Roman and early medieval periods: New data from  $^{226}\text{Ra}$ – $^{230}\text{Th}$  dating and archaeomagnetism. *Journal of Volcanology and Geothermal Research*, 304, 265–271. <https://doi.org/10.1016/j.jvolgeores.2015.09.002>
- Branca, S., De Beni, E., & Proietti, C. (2013). The large and destructive 1669 AD eruption at Etna volcano: Reconstruction of the lava flow field evolution and effusion rate trend. *Bulletin of Volcanology*, 75(2), 1–16. <https://doi.org/10.1007/s00445-013-0694-5>
- Branca, S., & Del Carlo, P. (2005). Types of eruptions of Etna volcano AD 1670–2003: Implications for short-term eruptive behaviour. *Bulletin of Volcanology*, 67(8), 732–742. <https://doi.org/10.1007/s00445-005-0412-z>

- Branca, S., Privitera, F., Palio, O., & Turco, M. (2021). Prehistoric human presence on Mount Etna (Sicily), in relation to the geological evolution. *Annals of Geophysics*, 64(5), VO542. <https://doi.org/10.4401/ag-8667>
- Brown, L., & Mertzman, S. A. (1979). Negative inclination anomalies from the Medicine Lake Highland lavas, northern California. *Earth and Planetary Science Letters*, 42(1), 121–126. [https://doi.org/10.1016/0012-821X\(79\)90197-3](https://doi.org/10.1016/0012-821X(79)90197-3)
- Brunns, M., Levin, I., Münnich, K. O., Hubberten, H. W., & Fillipakis, S. (1980). Regional sources of volcanic carbon dioxide and their influence on  $^{14}\text{C}$  content of present-day plant material. *Radiocarbon*, 22(2), 532–536. <https://doi.org/10.1017/S0033822200009851>
- Calvari, S., Branca, S., Corsaro, R. A., De Beni, E., Miraglia, L., Norini, G., et al. (2011). Reconstruction of the eruptive activity on the NE sector of Stromboli volcano: Timing of flank eruptions since 15 ka. *Bulletin of Volcanology*, 73(1), 101–112. <https://doi.org/10.1007/s00445-010-0412-5>
- Calvari, S., & Groppelli, G. (1996). Relevance of the Chiancone volcanioclastic deposit in the recent history of Etna Volcano (Italy). *Journal of Volcanology and Geothermal Research*, 72(3–4), 239–258. [https://doi.org/10.1016/0377-0273\(96\)00012-1](https://doi.org/10.1016/0377-0273(96)00012-1)
- Carracedo, J. C., Badiola, E. R., Guillou, H., Patrén, M., Scaillet, S., Torrado, F. P., et al. (2007). Eruptive and structural history of Teide Volcano and rift zones of Tenerife, Canary Islands. *Geological Society of America Bulletin*, 119(9–10), 1027–1051. <https://doi.org/10.1130/B26087.1>
- Carracedo, J. C., Troll, V. R., Day, J. M., Geiger, H., Aulinás, M., Soler, V., et al. (2022). The 2021 eruption of the cumbre vieja volcanic ridge on la palma, canary islands. *Geology Today*, 38(3), 94–107. <https://doi.org/10.1111/gto.12388>
- Carrancho, Á., Villalafán, J. J., Pavón-Carrasco, F. J., Osete, M. L., Straus, L. G., Vergès, J. M., et al. (2013). First directional European paleosecular variation curve for the Neolithic based on archaeomagnetic data. *Earth and Planetary Science Letters*, 380, 124–137. <https://doi.org/10.1016/j.epsl.2013.08.031>
- Castro, J., & Brown, L. (1987). Shallow paleomagnetic directions from historic lava flows, Hawaii. *Geophysical Research Letters*, 14(12), 1203–1206. <https://doi.org/10.1029/GL014012p01203>
- Chadima, M. (2006). Remasoft 3.0 a user-friendly paleomagnetic data browser and analyzer [Software]. *Travaux Géophysiques*, 27, 20. <https://www.agico.com/text/software/remasoft.php>
- Chadima, M., & Hrouda, F. (2012). Thermomagnetic curve browser [Software]. AGICO. <https://www.agico.com/text/software/cureval/cureval.php>
- Chevallier, R. (1925). L'aimantation des laves de l'Etna et l'orientaton du champ ocalizat en Sicile du XII au XVII ocali. *Annals of Physics*, 4, 5–162.
- Christie, M. (2018). Radiocarbon dating. *WikiJournal of Science*, 1(1), 1–17. <https://doi.org/10.15347/wjs/2018.006>
- Coltellini, M., Del Carlo, P., & Vezzoli, L. (1998). Discovery of a Plinian basaltic eruption of Roman age at Etna volcano, Italy. *Geology*, 26(12), 1095–1098. [https://doi.org/10.1130/0091-7613\(1998\)026<1095:DOAPBE>2.3.CO;2](https://doi.org/10.1130/0091-7613(1998)026<1095:DOAPBE>2.3.CO;2)
- Coltellini, M., Del Carlo, P., & Vezzoli, L. (2000). Stratigraphic constraints for explosive activity in the past 100 ka at Etna Volcano, Italy. *International Journal of Earth Sciences*, 89(3), 665–677. <https://doi.org/10.1007/s005310000117>
- Connor, C., Bebbington, M., & Marzocchi, W. (2015). Probabilistic volcanic hazard assessment. In *The encyclopedia of volcanoes* (pp. 897–910). Academic Press. <https://doi.org/10.1016/B978-0-12-385938-9.00051-1>
- Constable, C., Korte, M., & Panovska, S. (2016). Persistent high paleosecular variation activity in southern hemisphere for at least 10 000 years. *Earth and Planetary Science Letters*, 453, 78–86. <https://doi.org/10.1016/j.epsl.2016.08.015>
- Corkill, R. M., & Turner, G. M. (2022). A Holocene paleomagnetic secular variation record from Lake Pupuke, New Zealand. *New Zealand Journal of Geology and Geophysics*, 65(4), 582–594. <https://doi.org/10.1080/00288306.2021.1985529>
- Corsaro, R. A., & Pompilio, M. (2004). Dynamics of magmas at Mount Etna. *Geophysical Monograph – American Geophysical Union*, 143, 91–110. <https://doi.org/10.1029/143gm07>
- De Beni, E., Branca, S., Coltellini, M., Groppelli, G., & Wijbrans, J. R. (2011).  $^{40}\text{Ar}/^{39}\text{Ar}$  isotopic dating of Etna volcanic succession. *Italian Journal of Geosciences*, 130(3), 292–305. <https://doi.org/10.3301/IJG.2011.14>
- De Beni, E., Cantarero, M., Neri, M., & Messina, A. (2021). Lava flows of Mt Etna, Italy: The 2019 eruption within the context of the last two decades (1999–2019). *Journal of Maps*, 17(3), 65–76. <https://doi.org/10.1080/17445647.2020.1854131>
- Di Chiara, A., Speranza, F., & Porreca, M. (2012). Paleomagnetic secular variation at the Azores during the last 3 ka. *Journal of Geophysical Research*, 117(B7), B07101. <https://doi.org/10.1029/2012JB009285>
- Di Chiara, A., Speranza, F., Porreca, M., Pimentel, A., D'Ajello Caracciolo, F., & Pacheco, J. (2014). Constraining chronology and time-space evolution of Holocene volcanic activity on the Capelo Peninsula (Faial Island, Azores): The paleomagnetic contribution. *Geological Society of America Bulletin*, 126(9–10), 1164–1180. <https://doi.org/10.1130/B30933.1>
- Di Fiore, F., Vona, A., Scarani, A., Giordano, G., Romano, C., Giordano, D., et al. (2023). Experimental constraints on the rheology of lavas from 2021 Cumbre Vieja eruption (La Palma, Spain). *Geophysical Research Letters*, 50(4), e2022GL100970. <https://doi.org/10.1029/2022GL100970>
- Doell, R. R., & Cox, A. (1963). The accuracy of the paleomagnetic method as evaluated from historic Hawaiian lava flows. *Journal of Geophysical Research*, 68(7), 1997–2009. <https://doi.org/10.1029/JZ068i007p01997>
- Dunlop, D. J., & Özdemir, O. (2001). *Rock magnetism: Fundamentals and frontiers* (p. 573). Cambridge University Press.
- Fisher, R. A. (1953). Dispersion on a sphere. *Proceedings of the Royal Society of London. Series A. Mathematical and Physical Sciences*, 217(1130), 295–305. <https://doi.org/10.1098/rspa.1953.0064>
- Gallet, Y., Genevey, A., & Le Goff, M. (2002). Three millennia of directional variation of the Earth's magnetic field in Western Europe as revealed by archeological artefacts. *Physics of the Earth and Planetary Interiors*, 131(1), 81–89. [https://doi.org/10.1016/S0031-9201\(02\)00030-4](https://doi.org/10.1016/S0031-9201(02)00030-4)
- Gonzalez, S., Sherwood, G., Böhnel, H., & Schnepf, E. (1997). Palaeosecular variation in Central Mexico over the last 30000 years: The record from lavas. *Geophysical Journal International*, 130(1), 201–219. <https://doi.org/10.1111/j.1365-246X.1997.tb00999.x>
- Greve, A., & Turner, G. M. (2017). New and revised palaeomagnetic secular variation records from post-glacial volcanic materials in New Zealand. *Physics of the Earth and Planetary Interiors*, 269, 1–17. <https://doi.org/10.1016/j.pepi.2017.05.009>
- Greve, A., Turner, G. M., Conway, C. E., Townsend, D. B., Gamble, J. A., & Leonard, G. S. (2016). Palaeomagnetic refinement of the eruption ages of Holocene lava flows, and implications for the eruptive history of the Tongariro Volcanic Centre, New Zealand. *Geophysical Supplements to the Monthly Notices of the Royal Astronomical Society*, 207(2), 702–718. <https://doi.org/10.1093/gji/ggw296>
- Hagstrum, J. T., & Champion, D. E. (1994). Paleomagnetic correlation of Late Quaternary lava flows in the lower east rift zone of Kilauea Volcano, Hawaii. *Journal of Geophysical Research*, 99(B11), 21679–21690. <https://doi.org/10.1029/94JB01852>
- Holcomb, R., Champion, D., & McWilliams, M. (1986). Dating recent Hawaiian lava flows using paleomagnetic secular variation. *Geological Society of America Bulletin*, 97(7), 829–839. [https://doi.org/10.1130/0016-7606\(1986\)97<829:DRHLFU>2.0.CO;2](https://doi.org/10.1130/0016-7606(1986)97<829:DRHLFU>2.0.CO;2)

- Incoronato, A., Angelino, A., Romano, R., Romano, A., Sauna, R., Vanacore, G., & Vecchione, C. (2002). Retrieving geomagnetic secular variations from lava flows: Evidence from Mounts Arso, Etna and Vesuvius (southern Italy). *Geophysical Journal International*, 149(3), 724–730. <https://doi.org/10.1046/j.1365-246X.2002.01672.x>
- Jenkins, S. F., Phillips, J. C., Price, R., Feloy, K., Baxter, P. J., Hadmoko, D. S., & de Bélizal, E. (2015). Developing building-damage scales for lahars: Application to Merapi volcano, Indonesia. *Bulletin of Volcanology*, 77(9), 1–17. <https://doi.org/10.1007/s00445-015-0961-8>
- Juárez-Arriaga, E., Böhnel, H., Carrasco-Núñez, G., & Mahgoub, A. N. (2018). Paleomagnetism of Holocene lava flows from Los Humeros caldera, eastern Mexico: Discrimination of volcanic eruptions and their age dating. *Journal of South American Earth Sciences*, 88, 736–748. <https://doi.org/10.1016/j.jsames.2018.10.008>
- Jurado-Chichay, Z., Urrutia-Fucugauchi, J., & Rowland, S. K. (1996). A paleomagnetic study of the Pohue Bay flow and its associated coastal cones, Mauna Loa volcano, Hawaii: Constraints on their origin and temporal relationships. *Physics of the Earth and Planetary Interiors*, 97(1–4), 269–277. [https://doi.org/10.1016/0031-9201\(95\)03135-9](https://doi.org/10.1016/0031-9201(95)03135-9)
- Kirschvink, J. L. (1980). The least squares line and plane and the analysis of paleomagnetic data. *Geophysical Journal International*, 62(3), 699–718. <https://doi.org/10.1111/j.1365-246X.1980.tb02601.x>
- Knudsen, M. F., Jacobsen, B. H., & Abrahamsen, N. (2003). Palaeomagnetic distortion modelling and possible recovery by inversion. *Physics of the Earth and Planetary Interiors*, 135(1), 55–73. [https://doi.org/10.1016/S0031-9201\(02\)00203-0](https://doi.org/10.1016/S0031-9201(02)00203-0)
- Komorowski, J. C. (2002). The January 2002 eruption–The January 2002 flank eruption of Nyiragongo Volcano (Democratic Republic of Congo): Chronology, evidence for a tectonic rift trigger, and impact of lava flows on the city of Goma. *Acta ocalizationl: Journal of the National Volcanic Group of Italy*, 14(1–2), 27–62. <https://doi.org/10.1400/19077>
- Kono, M. (2015). Geomagnetism: An introduction and overview. Chapter 5. In G. Schubert (Ed.), *Treatise on geophysics*. Elsevier.
- Kovacheva, M., Kostadinova-Avramova, M., Jordanova, N., Lanos, P., & Boyadzhiev, Y. (2014). Extended and revised archaeomagnetic database and secular variation curves from Bulgaria for the last eight millennia. *Physics of the Earth and Planetary Interiors*, 236, 79–94. <https://doi.org/10.1016/j.pepi.2014.07.002>
- Krauskopf, K. B. (1948a). Lava movement at Paricutin volcano, Mexico. *Geological Society of America Bulletin*, 59(12), 1267–1284. [https://doi.org/10.1130/0016-7606\(1948\)59\[1267:LMAPVM\]2.0.CO;2](https://doi.org/10.1130/0016-7606(1948)59[1267:LMAPVM]2.0.CO;2)
- Krauskopf, K. B. (1948b). Mechanism of eruption at Paricutin volcano, Mexico. *Geological Society of America Bulletin*, 59(8), 711–732. [https://doi.org/10.1130/0016-7606\(1948\)59\[711:MOEAPV\]2.0.CO;2](https://doi.org/10.1130/0016-7606(1948)59[711:MOEAPV]2.0.CO;2)
- Lanos, P. (2004). Bayesian inference of calibration curves: Application to archaeomagnetism. In *Tools for constructing chronologies: Crossing disciplinary boundaries* (pp. 43–82). Springer London. [https://doi.org/10.1007/978-1-4471-0231-1\\_3](https://doi.org/10.1007/978-1-4471-0231-1_3)
- Lanza, R., Meloni, A., & Tema, E. (2005a). Historical measurements of the Earth's magnetic field compared with remanence directions from lava flows in Italy over the last four centuries. *Physics of the Earth and Planetary Interiors*, 148(1), 97–107. <https://doi.org/10.1016/j.pepi.2004.08.005>
- Lanza, R., Meloni, A., & Tema, E. (2005b). Reply to comment on “Historical measurements of the Earth's magnetic field compared with remanence directions from lava flows in Italy over the last four centuries”, by Tanguy, J. C., Principe, C., & Arrighi, S. *Physics of the Earth and Planetary Interiors*, 152(1–2), 121–124. <https://doi.org/10.1016/j.pepi.2005.05.001>
- Lanza, R., & Zanella, E. (2003). Paleomagnetic secular variation at Vulcano (Aeolian Islands) during the last 135 kyr. *Earth and Planetary Science Letters*, 213(3–4), 321–336. [https://doi.org/10.1016/S0012-821X\(03\)00326-1](https://doi.org/10.1016/S0012-821X(03)00326-1)
- Lanza, R., & Zanella, E. (2006). Comments on “chronology of vesuvius” activity from AD 79 to 1631 based on archeomagnetism of lavas and historical sources” by Principe, C., Tanguy, J. C., Arrighi, S., Paiotti, A., Goff, M. L., & Zoppi, U. *Bulletin of Volcanology*, 68(4), 394–396. <https://doi.org/10.1007/s00445-005-0030-9>
- Magli, A., Branca, S., Speranza, F., Risica, G., Siravo, G., & Giordano, G. (2022). Paleomagnetic dating of prehistoric lava flows from the urban district of Catania (Etna volcano, Italy). *Geological Society of America Bulletin*, 134(3–4), 616–628. <https://doi.org/10.1130/B36026.1>
- Magli, A., Speranza, F., Branca, S., Corsaro, R. A., Coltellini, M., Malaguti, A. B., & Giordano, G. (2023). Testing paleomagnetic dating accuracy on pre-historic flank eruptions from SE slope of Etna volcano [Dataset]. Zenodo. <https://doi.org/10.5281/zenodo.10143511>
- Mahgoub, A. N., Böhnel, H., Siebe, C., & Chevrel, M. O. (2017). Paleomagnetic study of El Metate shield volcano (Michoacán, Mexico) confirms its monogenetic nature and young age (~1250 CE). *Journal of Volcanology and Geothermal Research*, 336, 209–218. <https://doi.org/10.1016/j.jvolgeores.2017.02.024>
- Mahgoub, A. N., Böhnel, H., Siebe, C., Salinas, S., & Guibal, M. N. (2017). Paleomagnetically inferred ages of a cluster of Holocene monogenetic eruptions in the Tacámbaro–Puruarán area (Michoacán, México): Implications for volcanic hazards. *Journal of Volcanology and Geothermal Research*, 347, 360–370. <https://doi.org/10.1016/j.jvolgeores.2017.10.004>
- Mahgoub, A. N., Reyes-Guzmán, N., Böhnel, H., Siebe, C., Pereira, G., & Dorison, A. (2018). Paleomagnetic constraints on the ages of the Holocene Malpaís de Zacapu lava flow eruptions, Michoacán (Mexico): Implications for archeology and volcanic hazards. *The Holocene*, 28(2), 229–245. <https://doi.org/10.1177/0959683617721323>
- Malaguti, A. B., Branca, S., Speranza, F., Coltellini, M., Del Carlo, P., & Renzulli, A. (2023). Age of the Valle del Bove formation and chronology of the post-collapse flank eruptions, Etna volcano (Italy). *Journal of Volcanology and Geothermal Research*, 434, 107752. <https://doi.org/10.1016/j.jvolgeores.2023.107752>
- Malaguti, A. B., Rosi, M., Pistolesi, M., Speranza, F., & Menzies, M. (2022). The contribution of paleomagnetism, tephrochronology and radiocarbon dating to refine the last 1100 years of eruptive activity at Vulcano (Italy). *Bulletin of Volcanology*, 84(1), 1–19. <https://doi.org/10.1007/s00445-021-01515-7>
- Meredith, E. S., Jenkins, S. F., Hayes, J. L., Deligne, N. I., Lallemand, D., Patrick, M., & Neal, C. (2022). Damage assessment for the 2018 lower East Rift Zone lava flows of Kīlauea volcano, Hawai‘i. *Bulletin of Volcanology*, 84(7), 65. <https://doi.org/10.1007/s00445-022-01568-2>
- Molina-Cardín, A., Campuzano, S. A., Osete, M. L., Rivero-Montero, M., Pavón-Carrasco, F. J., Palencia-Ortas, A., et al. (2018). Updated Iberian archeomagnetic catalogue: New full vector paleosecular variation curve for the last three millennia. *Geochemistry, Geophysics, Geosystems*, 19(10), 3637–3656. <https://doi.org/10.1029/2018GC007781>
- Neal, C. A., Brantley, S. R., Antolik, L., Babb, J. L., Burgess, M., Calles, K., et al. (2019). The 2018 rift eruption and summit collapse of Kīlauea Volcano. *Science*, 363(6425), 367–374. <https://doi.org/10.1126/science.aav7046>
- Nilsson, A., Holme, R., Korte, M., Sutte, N., & Hill, M. (2014). Reconstructing Holocene geomagnetic field variation: New methods, models and implications. *Geophysical Journal International*, 198(1), 229–248. <https://doi.org/10.1093/gji/ggu120>
- Pasquier-Cardin, A., Allard, P., Ferreira, T., Hatte, C., Coutinho, R., Fontugne, M., & Jaudon, M. (1999). Magma-derived CO<sub>2</sub> emissions recorded in <sup>14</sup>C and <sup>13</sup>C content of plants growing in Furnas caldera, Azores. *Journal of Volcanology and Geothermal Research*, 92(1–2), 195–207. [https://doi.org/10.1016/S0377-0273\(99\)00076-1](https://doi.org/10.1016/S0377-0273(99)00076-1)
- Patrick, M. R., Dietterich, H. R., Lyons, J. J., Diefenbach, A. K., Parcheta, C., Anderson, K. R., et al. (2019). Cyclic lava effusion during the 2018 eruption of Kīlauea Volcano. *Science*, 366(6470), eaay9070. <https://doi.org/10.1126/science.aay9070>

- Pavón-Carrasco, F. J., Campuzano, S. A., Rivero-Montero, M., Molina-Cardín, A., Gómez-Paccard, M., & Osete, M. L. (2021). SCHA. DIF. 4k: 4,000 years of paleomagnetic reconstruction for Europe and its application for dating. *Journal of Geophysical Research: Solid Earth*, 126(3), e2020JB021237. <https://doi.org/10.1029/2020JB021237>
- Pavón-Carrasco, F. J., Osete, M. L., Torta, J. M., & De Santis, A. (2014). A geomagnetic field model for the Holocene based on archaeomagnetic and lava flow data. *Earth and Planetary Science Letters*, 388, 98–109. <https://doi.org/10.1016/j.epsl.2013.11.046>
- Pavón-Carrasco, F. J., Rodríguez-González, J., Osete, M. L., & Torta, J. M. (2011). A Matlab tool for archaeomagnetic dating. *Journal of Archaeological Science*, 38(2), 408–419. <https://doi.org/10.1016/j.jas.2010.09.021>
- Pavón-Carrasco, F. J., & Villasante-Marcos, V. (2010). Geomagnetic secular variation in the canary islands: Paleomagnetic data, models and application to paleomagnetic dating. *Física de la Tierra*, 2010(22), 59–80.
- Petrovský, E., & Kapička, A. (2006). On determination of the Curie point from thermomagnetic curves. *Journal of Geophysical Research*, 111(B12), B12S27. <https://doi.org/10.1029/2006JB004507>
- Pinton, A., Giordano, G., Speranza, F., & Þórðarson, P. (2018). Paleomagnetism of Holocene lava flows from the Reykjanes Peninsula and the Tungnáa lava sequence (Iceland): Implications for flow correlation and ages. *Bulletin of Volcanology*, 80(1), 1–9. <https://doi.org/10.1007/s00445-017-1187-8>
- Quidelleur, X., Gillot, P. Y., Filoche, G., & Lefèvre, J. C. (2005). Fast geochemical changes and rapid lava accumulation at Stromboli Island (Italy) inferred from K–Ar dating and paleomagnetic variations recorded at 60 and 40 ka. *Journal of Volcanology and Geothermal Research*, 141(3–4), 177–193. <https://doi.org/10.1016/j.jvolgeores.2004.10.004>
- Reimer, P. J., Austin, W. E., Bard, E., Bayliss, A., Blackwell, P. G., Ramsey, C. B., et al. (2020). The IntCal20 Northern Hemisphere radiocarbon age calibration curve (0–55 cal kBP). *Radiocarbon*, 62(4), 725–757. <https://doi.org/10.1017/RDC.2020.41>
- Renne, P. R., Sharp, W. D., Deino, A. L., Orsi, G., & Civetta, L. (1997).  $^{40}\text{Ar}/^{39}\text{Ar}$  dating into the historical realm: Calibration against Pliny the Younger. *Science*, 277(5330), 1279–1280. <https://doi.org/10.1126/science.277.5330.1279>
- Risica, G., Di Roberto, A., Speranza, F., Del Carlo, P., Pompilio, M., Meletlidis, S., & Rosi, M. (2020). Refining the Holocene eruptive activity at Tenerife (Canary Islands): The contribution of palaeomagnetism. *Journal of Volcanology and Geothermal Research*, 401, 106930. <https://doi.org/10.1016/j.jvolgeores.2020.106930>
- Risica, G., Di Roberto, A., Speranza, F., Del Carlo, P., Pompilio, M., Meletlidis, S., & Todrani, A. (2022). Reconstruction of the subaerial Holocene volcanic activity through paleomagnetic and  $^{14}\text{C}$  dating methods: El Hierro (Canary Islands). *Journal of Volcanology and Geothermal Research*, 425, 107526. <https://doi.org/10.1016/j.jvolgeores.2022.107526>
- Risica, G., Speranza, F., Giordano, G., De Astis, G., & Lucchi, F. (2019). Palaeomagnetic dating of the Neostromboli succession. *Journal of Volcanology and Geothermal Research*, 371, 229–244. <https://doi.org/10.1016/j.jvolgeores.2018.12.009>
- Rivero-Montero, M., Gómez-Paccard, M., Kondopoulou, D., Tema, E., Pavón-Carrasco, F. J., Aidona, E., et al. (2021). Geomagnetic field intensity changes in the Central Mediterranean between 1500 BCE and 150 CE: Implications for the levantine iron age anomaly evolution. *Earth and Planetary Science Letters*, 557, 116732. <https://doi.org/10.1016/j.epsl.2020.116732>
- Rivero-Montero, M., Gómez-Paccard, M., Pavón-Carrasco, F. J., Cau-Ontiveros, M. A., Fantuzzi, L., Martín-Hernández, F., et al. (2021). Refining geomagnetic field intensity changes in Europe between 200 CE and 1800 CE. New data from the Mediterranean region. *Physics of the Earth and Planetary Interiors*, 317, 106749. <https://doi.org/10.1016/j.pepi.2021.106749>
- Robertson, D. J. (1986). A paleomagnetic study of Rangitoto Island, Auckland, New Zealand. *New Zealand Journal of Geology and Geophysics*, 29(4), 405–411. <https://doi.org/10.1080/00288306.1986.10422162>
- Rolph, T. C., & Shaw, J. (1986). Variations of the geomagnetic field in Sicily. *Journal of Geomagnetism and Geoelectricity*, 38(12), 1269–1277. <https://doi.org/10.5636/jgg.38.1269>
- Roperch, P., Chauvin, A., Lara, L. E., & Moreno, H. (2015). Secular variation of the Earth's magnetic field and application to paleomagnetic dating of historical lava flows in Chile. *Physics of the Earth and Planetary Interiors*, 242, 65–78. <https://doi.org/10.1016/j.pepi.2015.03.005>
- Saupe, F., Strappa, O., Coppens, R., Guillet, B., & Jaegy, R. (1980). A possible source of error in  $^{14}\text{C}$  dates: Volcanic emanations (examples from the Monte Amiata district, provinces of Grosseto and Sienna, Italy). *Radiocarbon*, 22(2), 525–531. <https://doi.org/10.1017/S00382220000984X>
- Schanner, M., Korte, M., & Holschneider, M. (2022). ArchKalmag14k: A kalman-filter based global geomagnetic model for the Holocene. *Journal of Geophysical Research: Solid Earth*, 127(2), e2021JB023166. <https://doi.org/10.1029/2021JB023166>
- Schneider, C. A., Rasband, W. S., & Eliceiri, K. W. (2012). NIH image to ImageJ: 25 years of image analysis. *Nature Methods*, 9(7), 671–675. <https://doi.org/10.1038/nmeth.2089>
- Selva, J., Acocella, V., Bisson, M., Caliro, S., Costa, A., Della Seta, M., et al. (2019). Multiple natural hazards at volcanic islands: A review for the Ischia volcano (Italy). *Journal of Applied Volcanology*, 8(1), 1–43. <https://doi.org/10.1186/s13617-019-0086-4>
- Smittarello, D., Smets, B., Barrière, J., Michellier, C., Oth, A., Shreve, T., et al. (2022). Precursor-free eruption triggered by edifice rupture at Nyiragongo volcano. *Nature*, 609(7925), 83–88. <https://doi.org/10.1038/s41586-022-05047-8>
- Speranza, F., Branca, S., Coltellini, M., D'Ajello Caracciolo, F., & Vigliotti, L. (2006). How accurate is “paleomagnetic dating”? New evidence from historical lavas from Mount Etna. *Journal of Geophysical Research*, 111(B12), B12S33. <https://doi.org/10.1029/2006JB004496>
- Speranza, F., Di Chiara, A., & Rotolo, S. G. (2012). Correlation of welded ignimbrites on Pantelleria (Strait of Sicily) using paleomagnetism. *Bulletin of Volcanology*, 74(2), 341–357. <https://doi.org/10.1007/s00445-011-0521-9>
- Speranza, F., Pompilio, M., D'Ajello Caracciolo, F., & Sagnotti, L. (2008). Holocene eruptive history of the Stromboli volcano: Constraints from paleomagnetic dating. *Journal of Geophysical Research*, 113(B9), B09101. <https://doi.org/10.1029/2007JB005139>
- Speranza, F., Pompilio, M., & Sagnotti, L. (2004). Paleomagnetism of spatter lavas from Stromboli volcano (Aeolian Islands, Italy): Implications for the age of paroxysmal eruptions. *Geophysical Research Letters*, 31(2), L02607. <https://doi.org/10.1029/2003GL018944>
- Speranza, F., Sagnotti, L., & Meloni, A. (2005). Comment on “Recent eruptive history of Stromboli (Aeolian Islands, Italy) determined from high-accuracy archaeomagnetic dating”. In S. Arribigh, M. Rosi, J. C. Tanguy, & V Courtillot. *Geophysical Research Letters*, 32(23), L23306. <https://doi.org/10.1029/2005GL022590>
- Stuiver, M., Reimer, P. J., & Reimer, R. W. (2021). CALIB 8.2 [Software]. CALIB. <http://calib.org/calib/>
- Takaoka, N. (1989). Problems in the K–Ar dating of Quaternary volcanic rocks younger than 1 Ma. *Shitsuryo Bunseki*, 37(6), 343–351. <https://doi.org/10.5702/massspec.37.343>
- Tanguy, J. C., Bucur, I., & Thompson, J. F. C. (1985). Geomagnetic secular variation in Sicily and revised ages of historic lavas from Mount Etna. *Nature*, 318(6045), 453–455. <https://doi.org/10.1038/3184530>
- Tanguy, J. C., Condomines, M., Branca, S., La Delfa, S., & Coltellini, M. (2012). New archeomagnetic and  $^{226}\text{Ra}$ – $^{230}\text{Th}$  dating of recent lavas for the Geological map of Etna volcano. *Italian Journal of Geosciences*, 131(2), 241–257. <https://doi.org/10.3301/IJG.2012.01>

- Tanguy, J. C., Condomines, M., Le Goff, M., Chillemi, V., La Delfa, S., & Patanè, G. (2007). Mount Etna eruptions of the last 2,750 years: Revised chronology and location through archeomagnetic and  $^{226}\text{Ra}$ - $^{230}\text{Th}$  dating. *Bulletin of Volcanology*, 70(1), 55–83. <https://doi.org/10.1007/s00445-007-0121-x>
- Tanguy, J. C., & Le Goff, M. (2004). Distortion of the geomagnetic field in volcanic terrains: An experimental study of the Mount Etna stratovolcano. *Physics of the Earth and Planetary Interiors*, 141(1), 59–70. <https://doi.org/10.1016/j.pepi.2003.10.003>
- Tanguy, J. C., Le Goff, M., Principe, C., Arrighi, S., Chillemi, V., Paiotti, A., et al. (2003). Archeomagnetic dating of Mediterranean volcanics of the last 2100 years: Validity and limits. *Earth and Planetary Science Letters*, 211(1–2), 111–124. [https://doi.org/10.1016/S0012-821X\(03\)00186-9](https://doi.org/10.1016/S0012-821X(03)00186-9)
- Tarquini, S., & Nannipieri, L. (2017). The 10 m-resolution TINITALY DEM as a trans-disciplinary basis for the analysis of the Italian territory: Current trends and new perspectives. *Geomorphology*, 281, 108–115. <https://doi.org/10.1016/j.geomorph.2016.12.022>
- Tedesco, D., Vaselli, O., Papale, P., Carn, S. A., Voltaggio, M., Sawyer, G. M., et al. (2007). January 2002 volcano-tectonic eruption of Nyiragongo volcano, Democratic Republic of Congo. *Journal of Geophysical Research*, 112(B9), B09202. <https://doi.org/10.1029/2006JB004762>
- Tema, E., & Lanos, P. (2021). New Italian directional and intensity archaeomagnetic reference curves for the past 3000 years: Insights on secular variation and implications on dating. *Archaeometry*, 63(2), 428–445. <https://doi.org/10.1111/arcm.12603>
- Thompson, R., & Turner, G. M. (1985). Icelandic Holocene paleolimnromagnetism. *Physics of the Earth and Planetary Interiors*, 38(4), 250–261. [https://doi.org/10.1016/0031-9201\(85\)90072-X](https://doi.org/10.1016/0031-9201(85)90072-X)
- Turner, G. M., & Thompson, R. (1981). Lake sediment record of the geomagnetic secular variation in Britain during Holocene times. *Geophysical Journal International*, 65(3), 703–725. <https://doi.org/10.1111/j.1365-246X.1981.tb04879.x>
- Turner, G. M., & Thompson, R. (1982). Detransformation of the British geomagnetic secular variation record for Holocene times. *Geophysical Journal International*, 70(3), 789–792. <https://doi.org/10.1111/j.1365-246X.1982.tb05983.x>
- Urrutia-Fucugauchi, J., Alva-Valdivia, L. M., Goguitchaichvili, A., Rivas, M. L., & Morales, J. (2004). Palaeomagnetic, rock-magnetic and microscopy studies of historic lava flows from the Paricutin volcano, Mexico: Implications for the deflection of palaeomagnetic directions. *Geophysical Journal International*, 156(3), 431–442. <https://doi.org/10.1111/j.1365-246X.2004.02166.x>
- Valet, J. P., & Soler, V. (1999). Magnetic anomalies of lava fields in the Canary Islands. Possible consequences for paleomagnetic records. *Physics of the Earth and Planetary Interiors*, 115(2), 109–118. [https://doi.org/10.1016/S0031-9201\(99\)00071-0](https://doi.org/10.1016/S0031-9201(99)00071-0)
- Villasante-Marcos, V., & Pavón-Carrasco, F. J. (2014). Palaeomagnetic constraints on the age of Lomo Negro volcanic eruption (El Hierro, Canary Islands). *Geophysical Journal International*, 199(3), 1497–1514. <https://doi.org/10.1093/gji/ggu346>
- Wijibrans, J., Schneider, B., Kuiper, K., Calvari, S., Branca, S., De Beni, E., et al. (2011).  $^{40}\text{Ar}/^{39}\text{Ar}$  geochronology of Holocene basalts; examples from Stromboli, Italy. *Quaternary Geochronology*, 6(2), 223–232. <https://doi.org/10.1016/j.quageo.2010.10.003>
- Zanella, E., De Astis, G., & Lanza, R. (2001). Palaeomagnetism of welded, pyroclastic-fall scoriae at Vulcano, Aeolian Archipelago. *Journal of Volcanology and Geothermal Research*, 107(1–3), 71–86. [https://doi.org/10.1016/S0377-0273\(00\)00298-5](https://doi.org/10.1016/S0377-0273(00)00298-5)
- Zanella, E., Gurioli, L., Chiari, G., Ciarallo, A., Cioni, R., De Carolis, E., & Lanza, R. (2000). Archaeomagnetic results from mural paintings and pyroclastic rocks in Pompeii and Herculaneum. *Physics of the Earth and Planetary Interiors*, 118(3–4), 227–240. [https://doi.org/10.1016/S0031-9201\(99\)00146-6](https://doi.org/10.1016/S0031-9201(99)00146-6)
- Zijderveld, J. D. A. (1967). AC demagnetization of rocks: Analysis of results. In D. W. Collinson, K. M. Creer, & S. K. Runcorn (Eds.), *Methods in paleomagnetism* (pp. 254–286). Elsevier.